University of Twente

faculty of engineering technology

Engineering Fluid Dynamics Group

Multi-Level Wave-Ray solution of the 2D-Helmholtz equation

D.F. van Eijkeren

December 2008

TS-074

Multi-Level Wave-Ray solution of the 2D-Helmholtz equation

Dirk van Eijkeren

December 11, 2008

Abstract

The Helmholtz equation for standing wave solutions plays an important role in linear acoustics. For standing waves, the amplitude of the wave is only space-dependent and time independent. The vibration of a string for instance is time dependent, the amplitude of the vibration however is only space dependent. The amplitude functions are combinations of harmonic functions, with a phase progress depending on the local wave-number.

The Helmholtz equation is often considered on (semi-)infinite domains subjected to radiation boundary conditions. An aircraft in the distance for instance, radiating noise to a populated area. This highly indefinite case, with a high wave-number relative to the domain, has solutions with a large number of sine and cosine periods. Solving this problem numerically requires a high number of points to represent all wave periods accurately.

Iterative techniques are used to obtain a numerical solution, but these are computationally expensive for problems with a large number of points. Generally, Multi-Level algorithms greatly increase the performance of iterative techniques. Standard Multi-Levelalgorithms, however, do not work properly for the discretized Helmholtz equation. A Wave-Ray algorithm, proposed by Livsthits and Brandt [1], not only restores the performance of the standard Multi-Level algorithm, it also facilitates, in natural fashion, incorporation of the radiation boundary conditions. Separation of rays is required for the algorithm to work.

Th Wave-Ray algorithm has found little application in acoustics so far. The objective of this research is to determine the potential of such an algorithm for acoustics. The target of this research is to determine the potential of the algorithm for acoustics. In this thesis a Wave-Ray algorithm is produced for the 1D-Helmholtz equation, for the non-homogeneous case with varying wave-number, using separation of Rays. Results show a major increase in performance with respect to standard iterative and Multi-Level techniques. For the 2D case a separation scheme is produced for eight ray-directions, and is for four directions, implemented in a Wave-Ray algorithm.

Samenvatting

De Helmholtz vergelijking speelt een belangrijke rol in de akoestiek. De vergelijking geeft de amplitude van de golf voor staande golven. Deze is alleen afhankelijk van de plaats in de ruimte, en onafhankelijk van de tijd. Dit is te zien in bijvoorbeeld het trillen van een snaar. De snaar trilt gedurende de tijd, maar de amplitude van deze trilling is alleen afhankelijk van de locatie op de snaar. De functie voor de amplitude is een combinatie van harmonische functies, waarbij de fase voortgang afhangt van het golfgetal.

De Helmholtz vergelijking wordt vaak beschouwt in (semi-)oneindige domeinen, waarbij op de randen geluid het domein in straalt. Bijvoorbeeld een vliegtuig ver weg, dat geluid naar een bewoond gebied uitstraalt. Oplossingen, voor een relatief groot golfgetal voor het gebied waarin het geluid zich voortplant, zullen veel periodes van de harmonische functies bevatten. Om zulke problemen numeriek op te lossen is vaak een zeer fijn rekenrooster nodig om alle golven nauwkeurig weer te geven. Omdat het rekengebied ook nog eens groot is, zijn dan zeer veel rekenpunten nodig.

Iteratieve technieken worden vaak gebruikt bij het verkrijgen van numerieke oplossingen. Deze technieken kosten echter veel computerkracht voor problemen met veel rekenpunten. Multi-Level algoritmes zullen over het algemeen de prestaties van de iteratieve technieken zeer verbeteren. De standaard Multi-Level technieken werken echter niet goed voor de gediscretiseerde Helmholtz vergelijking. Een Wave-Ray algoritme, voorgesteld door Livshits en Brandt [1], zou de prestaties van het Multi-Level algoritme moeten verbeteren. Het kan er ook voor zorgen dat het uitgestraalde geluid op een natuurlijke manier in de randvoorwaarden wordt verwerkt. Voor het algoritme is het nodig om de verschillende stralen te kunnen scheiden.

Tot op heden heeft het Wave-Ray algoritme weinig aandacht gekregen in de literatuur. Het doel van dit onderzoek is om de potentie van dit algoritme voor akoestische berekeningen te onderzoeken. Hiervoor is een Wave-Ray algoritme is ontwikkeld voor de gediscretiseerde 1D-Helmholtz vergelijking, voor het inhomogene geval met een varierend golfgetal, waarbij het scheiden van stralen wordt gebruikt. De resultaten laten zien dat het algoritme de prestaties van de standaard iteratieve en Multi-Level technieken zeer verbetert. Voor het 2D geval is een scheidings schema ontwikkeld voor het scheiden van acht straalrichtingen. Dit schema is voor vier stralen in het Wave-Ray algoritme verwerkt.

Preface

This is a Master's thesis for my graduation project for the master programme Mechanical Engineering, followed at the department of Engineering Fluid Dynamics, on the University of Twente. I chose for the bachelor programme Werktuigbouwkunde (Mechanical Engineering), because I was interested in fluid dynamics. Two projects during the Bachelor related to this subject increased this interest. The tutor for project T, on the cooling of turbine stator blades, was my current supervisor Kees Venner. He was able to inspire us to derive the so called Integral Method for Boundary layers.

The work in this thesis is about developing an efficient solution method for the Helmholtz equation. It is a continuation of work done by Ellen van Emden on the one dimensional Helmholtz equation, and is based on work done by Ira Livshits on Multi-Level methods for the Helmholtz equation. I would like to thank them for providing the base, without which this thesis would not be possible.

Multi-Level methods got to my attention during the lectures of Kees Venner for the subject Computational Fluid Dynamics. I subsequently worked on the subject Multi-Level methods, focussed for summations and integral equations. Kees introduced the Helmholtz equation as a possibility for the Master's thesis. I would therefore like to thanks Kees, not only for supervising this research, but also for triggering the interest in this subject during his lectures and tutoring of project T.

I also would like to thank Prof. dr. ir. Harry Hoeijmakers, the head of the Engineering Fluid Dynamics, for his continuing interest and supervision of the master programme, and also for the comments on this work, sent to me, during the Student Tour for mechanical engineering, from Brazil by mail and e-mail.

I would also like to thank my colleagues in this department. In particular my current and former room mates for their support and for enduring my taste of music. Especially Sietse Jongsma, currently employed as AIO, for all the fun during the first half of the year and for commenting my texts. I also would like to specially thank Koen van Andel for all the jokes during my stay at the University of Twente.

Finally I would like to thank my house mates for their company, and my parents for their support and acceptance of my choice for Mechanical Engineering.

Contents

Chapter 1

Introduction

1.1 Acoustics

Acoustics is the science of sound. It is the domain in physics that deals with the generation and propagation of sound waves. The domain is most often divided into structural acoustics and aero-acoustics. Structural acoustics deals with the occurrence of vibrations in structures. For instance, the engine and propeller of a cruise ship cause disturbing vibrations of the chairs and tables in the ships restaurant. Aero-acoustics mostly deals with the occurrence of vibrations in fluids and more specifically air, e.g. the noise of a car driving past or the wind whistling through the crack of a window on a stormy day. Most often problems are not specifically aero- or structural acoustics. The vibrations in the ship for instance will also cause noise in the restaurant because of sound propagating through the air.

The prediction and control of sound is becoming an increasingly important subject. The level of acceptance of noise from vehicles, and mechanical and electrical machines and tools has decreased. Another reason for the interest in the accurate prediction and control of sound is the increasing need for realistic sound systems for films, music and computer games. With new techniques noise can either be decreased or radiated to a region where noise is not a problem. Models have to be developed for the prediction and control of sound. Solving the modelling equations often involves numerical simulations with computers.

Some models are only accurate for specific cases and therefore a classification of the problems is needed. Acoustics can mainly be divided into internal and external acoustics. In interior acoustics the domain is bounded by solid surfaces such as a room or a cabin. In external acoustics the domain is, at least partly, unbounded. For instance, the sound radiated from an aircraft to the surroundings. For both types of problems different methods and models have been developed, in order to be able to, most optimally, solve the specific problems.

1.2 The Helmholtz equation

The Helmholtz equation is used in linear acoustics. It describes the propagation of small perturbations in a medium. The Helmholtz equation is obtained from the equations for conservation of mass, momentum and energy used in fluid dynamics by assuming linear perturbations. In a control volume mass, momentum and energy can change in time. One cause for the change of such a quantity is transport through the boundary of the volume. The second cause is the production or destruction of a quantity inside the volume, for instance, a chemical reaction producing heat increases the energy in the volume.

The conservation equations are integral equations and they only give a global solution for the interior of the volume. To obtain detailed solutions for the interior of a volume the conservation equations are generally expressed in terms of partial differential equations (PDE's). The equation of conservation of mass in PDE form is:

$$\frac{\partial \rho}{\partial t} + \frac{\partial \rho u_j}{\partial x_j} = 0 \tag{1.1}$$

with ρ the local density, in $\left[\mathrm{kg\,m^{-3}}\right]$, and $\mathbf{u}$ the local flow velocity vector in $\left[\mathrm{m\,s^{-1}}\right]$.

Conservation of momentum leads to:

$$\frac{\partial \rho u_i}{\partial t} + \frac{\partial \rho u_i u_j}{\partial x_j} = -\frac{\partial p}{\partial x_i} + F_i + \frac{\partial \tau_{ij}}{\partial x_j} \tag{1.2}$$

with p the local pressure in the fluid, in $\left[\mathrm{N\,m^{-2}}\right]$, $\mathbf{F}$ the density of the force field vector, in $\left[\mathrm{N\,m^{-3}}\right]$, acting in the bulk of the fluid and τ_{ij} the viscous stress tensor, in $\left[\mathrm{N\,m^{-2}}\right]$, which, for a Newtonian fluid, is given by:

$$\tau_{ij} = \mu\left(\frac{\partial u_i}{\partial x_j} + \frac{\partial u_j}{\partial x_i}\right) + \lambda\delta_{ij}\frac{\partial u_k}{\partial x_k} \tag{1.3}$$

Conservation of energy can be expressed as:

$$\frac{\partial \rho E}{\partial t} + \frac{\partial \rho E u_j}{\partial x_j} = -\frac{\partial p u_j}{\partial x_j} + F_i u_i + \frac{\partial \tau_{ij} u_i}{\partial x_j} + \dot{Q} - \frac{\partial q_j}{\partial x_j} \tag{1.4}$$

with E the local total energy per unit mass of the fluid, in $\left[\mathrm{J\,kg^{-1}}\right]$, $\dot{Q}$ the time rate of volumetric heat addition, in $\left[\mathrm{J\,m^{-3}s^{-1}}\right]$, and $\mathbf{q}$ is the heat flux vector, in $\left[\mathrm{J\,m^{-2}s^{-1}}\right]$.

For the derivation of the Helmholtz equation it will be assumed that viscous and heat conduction effects can be neglected. Furthermore the flow is assumed to be adiabatic, i.e. $\dot{Q} = 0$. Furthermore, it is assumed that very small perturbations in velocity, pressure and density $\mathbf{u}'$, p' and ρ' act on their

respective reference states $\mathbf{u}_0$, p_0 and ρ_0 such that $\mathbf{u} = \mathbf{u}_0 + \mathbf{u}'$, $p = p_0 + p'$ and $\rho = \rho_0 + \rho'$ under the influence of small perturbations in the density of the force field $\mathbf{F}'$ acting on its reference state $\mathbf{F}_0$. The reference state itself is not necessarily constant in space, but is constant in time.

It is assumed that because of the small perturbations, and the negligible effects of viscosity and heat conduction as well as of non-adiabatic effects, the flow is isentropic. This implies the fluid flow is barotropic and therefore the pressure is a function of the density only. The barotropic relation relating the pressure perturbations and density perturbations then is:

$$p' = c_0^2 \rho' \tag{1.5}$$

where c_0 is the speed of sound in the reference state, and in a calorically perfect gas, such as air at room temperature,

$$c_0(\mathbf{x})^2 = \gamma \frac{p_0(\mathbf{x})}{\rho_0(\mathbf{x})} \tag{1.6}$$

with γ the ratio of the specific heats.

The reference state for the velocity will be chosen as $\mathbf{u}_0 = 0$. Substitution of the variables in the equation of mass conservation, neglecting quadratic and higher-order perturbation terms, gives:

$$\frac{\partial \rho'}{\partial t} + \rho_0 \frac{\partial u_i'}{\partial x_i} = 0 \tag{1.7}$$

From the equation for conservation of momentum, where the reference state for the force field will be chosen as $\mathbf{F}_0 = 0$, it follows that:

$$\rho_0 \frac{\partial u_i'}{\partial t} + \frac{\partial p'}{\partial x_i} = F_i' \tag{1.8}$$

The barotropic relation, 1.5, can now be substituted in 1.7 or 1.8 to either eliminate ρ', or p'. For each of the perturbations in p, ρ, or $\mathbf{u}$ a simple PDE is obtained. For example the PDE for the pressure variations thus obtained is:

$$\frac{1}{c_0^2} \frac{\partial^2 p'}{\partial t^2} - \frac{\partial^2 p'}{\partial x_i^2} = -\frac{\partial F_i'}{\partial x_i} \tag{1.9}$$

Separation of variables by assuming $p'(\mathbf{x}, t) = G(t) P(\mathbf{x})$ then leads to:

$$G \nabla^2 P = \frac{P}{c_0^2} \frac{d^2 G}{dt^2} + f(\mathbf{x}) g(t) \tag{1.10}$$

where $f g = -\frac{\partial F_i'}{\partial x_i}$ is the forcing.

In linearized systems, such as equation 1.8, the superposition principle can be used to combine solutions satisfying the homogeneous equation and part

of the inhomogeneous terms. Therefore, if the forcing is harmonic, e.g. a harmonically vibrating speaker, assuming the superposition principle, forcing functions and solutions can be decomposed in Fourier components leading to an equation for each Fourier component. The forcing function for a single Fourier component g can be written as:

$$g(t) = C_1 e^{\iota\omega t} \tag{1.11}$$

where ω the frequency of its Fourier component, in $\left[\mathrm{rad\,s^{-1}}\right]$, which does not depend on time nor space.

Solutions G can then be written as:

$$G(t) = C_2 e^{\iota\omega t} \tag{1.12}$$

with ω the same frequency as the forcing.

The variables C_1 and C_2, used in the functions, are constants in time and space. As C_1 and C_2 are constants and the general solution and forcing are multiplications of time and spatial functions they can be combined with their respective spatial functions without loss of generality. This leads to:

$$G(t) = e^{\iota\omega t} \tag{1.13}$$

and:

$$g(t) = e^{\iota\omega t} \tag{1.14}$$

Substitution, of this assumption on $G(t)$ and $g(t)$, in equation 1.10 gives:

$$\nabla^2 P e^{\iota\omega t} = -\frac{\omega^2}{c_0^2} P e^{\iota\omega t} + f e^{\iota\omega t} \tag{1.15}$$

Leading to the elimination of t from the equation:

$$\nabla^2 P = -\frac{\omega^2}{c_0^2} P + f \tag{1.16}$$

This is the Helmholtz equation:

$$\nabla^2 P(\mathbf{x}) + k^2(\mathbf{x}) P(\mathbf{x}) = f(\mathbf{x}) \tag{1.17}$$

with:

$$k^2(\mathbf{x}) = \frac{\omega^2}{c_0^2(\mathbf{x})} \tag{1.18}$$

As the pressure, the density and the velocity perturbations are related to each other, the Helmholtz equation is solved for one variable only.

The Helmholtz equation is an elliptic equation and therefore it can be solved if the boundary conditions are known along all boundaries. These conditions may differ for different parts of the boundary. One generally distinguishes

Dirichlet, Neumann, mixed or Robin, and Sommerfeld boundary conditions. However, with a Neumann condition on the entire boundary there is no unique solution, as it only forces the derivative on the boundary to have a certain value.

Only for some specific simplified cases, the Helmholtz equation can be solved analytically, e.g. a homogeneous one-dimensional problem with constant wave-number. In general a numerical approach is necessary. Several numerical methods are in use to solve differential equations numerically. For example, Finite Element Methods, which are more generally used in structural mechanics, use local shape functions to approximate the field variables. These functions will be linked on element boundaries and produce a system of algebraic equations that can be solved with standard techniques. Finite Element Methods are best suited for interior problems.

Another possible method is the Boundary Element Method(BEM), which is also called Panel Method in aerodynamics. On the boundary of the domain a distribution of elementary solutions is placed. For these distributions an integral equation can be obtained to determine their strength. With a known distribution the variables can be calculated in each point of the domain. Boundary Element Methods are useful when having large domains, as is the case for exterior problems. The reader is referred to [2] for a BEM Multi-Level Multi-Integration algorithm for acoustics. For both Finite Element Methods and Boundary Element Methods computation times can increase fast with increasing number of elements.

Another method to approximate solutions numerically is to use a Finite Difference Method. In Finite Difference Methods the differentials are approximated with a combination of Taylor series. These series are combined in such a way that the differential in a point can be expressed as a weighted sum of the values of the solution at nearby points. The accuracy of the approximation depends on the number of points and their location relative to the point at which the derivative is needed. An accuracy of $\mathcal{O}(h)$ and $\mathcal{O}\left(h^2\right)$ is easily obtained using very few neighbouring points on a grid with mesh size h. Higher order accuracy either requires more points or in addition to function values also derivatives as unknown solution parameters. These methods give detailed solutions and can be used for both exterior and interior problems. In this thesis a Finite Difference approximation will be used to solve the Helmholtz equation numerically.

The wave-number k determines the local frequency in space of the solution, e.g. with $k = 5\left[\mathrm{m}^{-1}\right]$ for a domain with $L = 2\pi\,[\mathrm{m}]$ the solution will be a wave function consisting of five periods. In the discretization each period requires a number of points in order to be able to represent the solution. Therefore the required mesh size decreases, and the required number of points increases, with increasing wave-number. The numerical scheme also introduces a phase error which accumulates during each period in the domain, and is of order $\mathcal{O}\left(Lk^3h^2\right)$ according to Livshits and Brandt [1]. This phase error can

therefore be reduced by using more point per period. Therefore, the mesh size, and thus the number of points, not only depends on the wave-number itself, but also of the wave-number relative to the total length of the domain.

The number of points needed in the entire domain is largely dependant on the combination of the wave-number and the size of the domain and can become very large when one or both of these are large. As the calculation time, for a numerical solution of the resulting system of equations, scales with $\mathcal{O}(n^\alpha)$, with n the number of points and $\alpha > 1$, the computing time, needed to obtain solutions on relatively large domains and relatively high k, will be very large. This situation is aggravated by the fact that many problems for which the Helmholtz equation has to be solved are considered in near infinite domains with radiation boundary conditions.

Multi-Level algorithms have been introduced as fast alternative methods for the numerical solution of problems in many fields of science. The standard approach for elliptic problems is to use an iterative process on a series of grids in a recursive manner to obtain a grid independent convergence rate. Therefore a fast solution can be obtained on the target grid. However, this standard approach fails for the Helmholtz equation in the highly indefinite case, e.g. large wave-number k and (semi-)infinite domains. For this case an extended algorithm, the Wave-Ray Multi-Level algorithm has been developed by Livshits and Brandt [1]. However, this algorithm has found little application in acoustics so far. The objective of this research is to determine the potential of such an algorithm for acoustics.

A wave-ray Multi-Level algorithm for the Helmholtz equation not only restores the performance of the standard Multi-Level algorithm, it also facilitates, in a natural fashion, incorporation of the radiation boundary conditions associated with these problems. It will require separation of the principal error components, the components that cause the standard Multi-Level approach to fail. In this thesis such a Multi-Level wave-ray algorithm will be developed for the one dimensional(1D) and the two dimensional(2D) case. An initial study to a Multi-Level wave-ray method for Finite Differences for the 1D case has been presented by Van Emden [3].

1.3 Objective

The objective of this thesis is to develop a Multi-Level algorithm along the lines suggested by Livshits and Brandt [1] for the highly indefinite 2D-Helmholtz equation, using a wave-ray algorithm. Steps taken to achieve this objective are:

- Extend a Multi-Level algorithm for the 1D-Helmholtz equation to be able to solve the non-homogeneous Helmholtz equation.
- Produce and show results of a scheme for separation of rays in 2D.

- Build a 2D-Wave-Ray algorithm using the separation scheme.
- Show results and analyse the performance of the Wave-Ray algorithm, for the 2D problem.

The work by E. van Emden on the 1D-Helmholtz equation is used as a starting point. This 1D-Helmholtz Wave-Ray algorithm will be extended to a Wave-Ray algorithm for the non-homogeneous 1D-Helmholtz equation. The 1D-Helmholtz Wave-Ray algorithm will then be used as a starting point for the 2D Wave-Ray algorithm along the lines suggested by Livshits and Brandt.

1.4 Outline

To be able to use a wave-ray algorithm some basic knowledge is required of analytical solutions satisfying the Helmholtz equation. In Chapter 2 these analytic solutions will be derived and will be used to determine an extra set of equations.

In Chapter 3 the numerical method will be discussed. First single grid Finite Difference Methods will be presented. Then the basic Multi-Level methodology will be explained. Its theoretical performance for the Helmholtz equation will be shown. Next the extension to the full Wave-Ray Multi-Level scheme is presented.

For the Wave-Ray algorithm it is necessary to be able to separate rays in a 2D-space. Chapter 4 will deal with this topic. Results will be shown to illustrate this method, in order to separate a combination of rays, resulting in a representation of eight separated rays.

In Chapter 5 results will be presented for the 1D Helmholtz equation. First the results for a standard iterative, and a standard Multi-Level approach will be presented for a simple case. Then results for the implementation of the wave-ray scheme will be presented for the same case, and the performances will be compared. Finally for several distinctive cases the wave-ray scheme will be used and the performance of the scheme will be discussed.

In Chapter 6 results will be presented for the implementaion of the 2D-Multi-Level wave-ray scheme. The performance of the scheme and the problems arising when using the scheme will be discussed.

Finally in Chapter 7 concluding remarks will be presented for the 1D and 2D wave-ray scheme and recommendations will be given for aspects that need to be researched further in order to finally produce a 3D Multi-Level wave-ray scheme for the 3D Helmholtz equation.

Chapter 2

Theory

In Section 1.2 the Helmholtz equation was derived for the spatial part of the pressure distribution, see equation 1.17. The equation will be written with a general variable u, as the Helmholtz equation can also be used to calculate e.g. the density or velocity perturbations:

$$\boldsymbol{\nabla}^2 u(\mathbf{x}) + k(\mathbf{x})^2 u(\mathbf{x}) = f(\mathbf{x}) \tag{2.1}$$

Analytic solutions are in most situations not easy to obtain. However, a formulation of general solution for this equation exists. For simple cases this general solution can be expressed as an exact solution. This exact solution can be used to show the accuracy of the solution obtained by the discretized equation. The general solution will later be used to reduce errors efficiently in the numerical approach and it is therefore necessary to introduce ray equations using the general solution.

For simplicity, the 1D-Helmholtz equation will be considered first. The Helmholtz equation is for standing waves and the solution gives the amplitude in each point of the vibration in time. General solutions for the Helmholtz equation are real and imaginary sine functions representing standing waves radiating in different directions. In 1D this will lead to:

$$u(x) = a(x)\, e^{\iota\left(s(x)+\varphi_a\right)} + b(x)\, e^{-\iota\left(s(x)+\varphi_b\right)} \tag{2.2}$$

with a and b the amplitude functions of the two possible ray-directions and s a function that describes the phase of the ray in the domain of interest. φ is a constant offset of the phase of the ray in the domain depending on both the boundary conditions for the rays radiated into the domain and s on the boundary.

For a constant wave-number however the analytic solution reduces to:

$$u(x) = a(x)\, e^{\iota\left(kx+\varphi_a\right)} + b(x)\, e^{-\iota\left(kx+\varphi_b\right)} \tag{2.3}$$

Therefore the local behaviour of the solution near location X is given by:

$$u(x) = a(X)\, e^{\iota\left(k(X)(x-X)+\varphi_{a,X}\right)} + b(X)\, e^{-\iota\left(k(X)(x-X)+\varphi_{b,X}\right)} \tag{2.4}$$

And thus:

$$u(X+\delta x) = a(X)\, e^{\iota\left(k(X)\delta x+\varphi_{a,X}\right)} + b(X)\, e^{-\iota\left(k(X)\delta x+\varphi_{b,X}\right)} \tag{2.5}$$

And also:

$$u(X+2\delta x) = a(X)\, e^{\iota\left(k(X)\delta x+k(X+\delta x)\delta x+\varphi_{a,X}\right)} + b(X)\, e^{-\iota\left(k(X)\delta x+k(X+\delta x)\delta x+\varphi_{b,X}\right)} \tag{2.6}$$

Expanding equations 2.4, 2.5 and 2.6 to the domain of the equation, s can be written as an infinite summation of $k\delta x$:

$$s(x) = \lim_{\delta x\to 0} \sum_{n=1}^{n=\frac{x}{\delta x}} k(n\delta x)\,\delta x \tag{2.7}$$

with n the index of the element with length δx, and, in the limit of δx to zero, going to infinity.

The limit of the summation can then be written as:

$$s(x) = \int_{x_0}^{x} k(x)\, dx \tag{2.8}$$

With the form of the analytic solution known, equations can be derived for $a(x)$ and $b(x)$. Substitution in the Helmholtz equation of the solution leads to:

$$\begin{aligned}\left(\frac{\mathrm{d}^2 a}{\mathrm{d}x^2} + \iota\left(\frac{\mathrm{d}s}{\mathrm{d}x}\frac{\mathrm{d}a}{\mathrm{d}x} + \frac{\mathrm{d}\left(\frac{\mathrm{d}s}{\mathrm{d}x}a\right)}{\mathrm{d}x}\right) + \left(k^2 - \left(\frac{\mathrm{d}s}{\mathrm{d}x}\right)^2\right)a\right) e^{\iota\left(s+\varphi_a\right)} \\ + \left(\frac{\mathrm{d}^2 b}{\mathrm{d}x^2} - \iota\left(\frac{\mathrm{d}s}{\mathrm{d}x}\frac{\mathrm{d}b}{\mathrm{d}x} + \frac{\mathrm{d}\left(\frac{\mathrm{d}s}{\mathrm{d}x}b\right)}{\mathrm{d}x}\right) + \left(k^2 - \left(\frac{\mathrm{d}s}{\mathrm{d}x}\right)^2\right)b\right) e^{-\iota\left(s+\varphi_b\right)} \\ = f_a e^{\iota\left(s+\varphi_a\right)} + f_b e^{-\iota\left(s+\varphi_b\right)}\end{aligned} \tag{2.9}$$

with:

$$f_a(x)\, e^{\iota\left(s+\varphi_a\right)} + f_b(x)\, e^{-\iota\left(s+\varphi_b\right)} = f \tag{2.10}$$

with k and f, not necessarily continuous, functions of x. Now, using equation 2.8 for s, the equation can be written as:

$$\begin{aligned}\left(\frac{\mathrm{d}^2 a}{\mathrm{d}x^2} + \iota\left(k\frac{\mathrm{d}a}{\mathrm{d}x} + \frac{\mathrm{d}(ka)}{\mathrm{d}x}\right)\right) e^{\iota\left(s+\varphi_a\right)} \\ + \left(\frac{\mathrm{d}^2 b}{\mathrm{d}x^2} - \iota\left(k\frac{\mathrm{d}b}{\mathrm{d}x} + \frac{\mathrm{d}(kb)}{\mathrm{d}x}\right)\right) e^{-\iota\left(s+\varphi_b\right)} \\ = f_a e^{\iota\left(s+\varphi_a\right)} + f_b e^{-\iota\left(s+\varphi_b\right)}\end{aligned} \tag{2.11}$$

Solutions for a and b that satisfy equation 2.11 can be written as:

$$a(x) = A_1(x) + A_2(x)\, e^{-2\iota s} \tag{2.12a}$$

$$b(x) = B_1(x) + B_2(x)\, e^{2\iota s} \tag{2.12b}$$

Where A_1, A_2, B_1 and B_2 are as smooth or smoother than a and b, and have to satisfy:

$$\begin{aligned}
&\left(\frac{\mathrm{d}^2\left(A_1 + A_2 e^{-2\iota s}\right)}{\mathrm{d}x^2} + \iota k \frac{\mathrm{d}\left(A_1 + A_2 e^{-2\iota s}\right)}{\mathrm{d}x} \right) e^{\iota(s+\varphi_a)} \\
&\quad + \iota \frac{\mathrm{d}\left(kA_1 + kA_2 e^{-2\iota s}\right)}{\mathrm{d}x} e^{\iota(s+\varphi_a)} + \frac{\mathrm{d}^2\left(B_1 + B_2 e^{2\iota s}\right)}{\mathrm{d}x^2} e^{-\iota(s+\varphi_b)} \\
&\quad - \iota \left(k \frac{\mathrm{d}B_1 + B_2 e^{2\iota s}}{\mathrm{d}x} + \frac{\mathrm{d}\left(kB_1 + kB_2 e^{2\iota s}\right)}{\mathrm{d}x} \right) e^{-\iota(s+\varphi_b)} \\
&\quad = f_a e^{\iota(s+\varphi_a)} + f_b e^{-\iota(s+\varphi_b)}
\end{aligned} \tag{2.13}$$

Rewriting the differential equations leads to a combination of differential equations like equation 2.11. However, as A_1, A_2, B_1 and B_2 are as smooth, or smoother than a and b, terms with $e^{\iota s}$ and with $e^{-\iota s}$ can be separated. This leads to:

$$\begin{aligned}
&\left(\frac{\mathrm{d}^2 A_1}{\mathrm{d}x^2} + \iota \left(k \frac{\mathrm{d}A_1}{\mathrm{d}x} + \frac{\mathrm{d}kA_1}{\mathrm{d}x} \right) \right) e^{\iota(s+\varphi_a)} \\
&\quad + \left(\frac{\mathrm{d}^2 B_2}{\mathrm{d}x^2} + \iota \left(k \frac{\mathrm{d}B_2}{\mathrm{d}x} + \frac{\mathrm{d}kB_2}{\mathrm{d}x} \right) \right) e^{\iota(s-\varphi_b)} \\
&\quad = f_a e^{\iota(s+\varphi_a)}
\end{aligned} \tag{2.14a}$$

$$\begin{aligned}
&\left(\frac{\mathrm{d}^2 A_2}{\mathrm{d}x^2} - \iota \left(k \frac{\mathrm{d}A_2}{\mathrm{d}x} + \frac{\mathrm{d}kA_2}{\mathrm{d}x} \right) \right) e^{-\iota(s-\varphi_a)} \\
&\quad + \left(\frac{\mathrm{d}^2 B_1}{\mathrm{d}x^2} - \iota \left(k \frac{\mathrm{d}B_1}{\mathrm{d}x} + \frac{\mathrm{d}kB_1}{\mathrm{d}x} \right) \right) e^{-\iota(s+\varphi_b)} \\
&\quad = f_b e^{-\iota(s+\varphi_b)}
\end{aligned} \tag{2.14b}$$

Terms with A_1 and B_2 both influence the same frequency in the solution of the Helmholtz equation, just as terms with A_2 and B_1. Therefore, boundary conditions can be chosen such that A_2 and B_2 are zero without loss of generality. These boundary conditions will be called the radiation boundary conditions (r.b.c.). From equations 2.12 with boundary conditions such that $A_2 = B_2 = 0$, equation 2.11 can be separated, leading to the so called ray-equations:

$$\frac{\mathrm{d}^2 a}{\mathrm{d}x^2} + \iota \left(\frac{\mathrm{d}ak}{\mathrm{d}x} + k \frac{\mathrm{d}a}{\mathrm{d}x} \right) = f_a \tag{2.15a}$$

$$\frac{\mathrm{d}^2 b}{\mathrm{d}x^2} - \iota\left(\frac{\mathrm{d}bk}{\mathrm{d}x} + k\frac{\mathrm{d}b}{\mathrm{d}x}\right) = f_b \tag{2.15b}$$

With radiation boundary conditions (r.b.c.):

$$a\left(x_a\right) = A \tag{2.16a}$$

$$\left.\frac{\mathrm{d}a}{\mathrm{d}x}\right|_{x_a} = 0 \tag{2.16b}$$

$$b\left(x_b\right) = B \tag{2.16c}$$

$$\left.\frac{\mathrm{d}b}{\mathrm{d}x}\right|_{x_b} = 0 \tag{2.16d}$$

with x_a the left and x_b the right boundary of the domain. For the homogeneous Helmholtz equation it might be preferable to solve the ray-equations instead of the Helmholtz equation. For the non-homogeneous Helmholtz equation however, the right hand side for the separate ray-equations is not known and therefore solutions cannot be determined. In the next Chapter it will be shown that the ray-equations can still be of use in increasing the speed of finding a solution of the Helmholtz equation for these cases.

For the 2D-Helmholtz equation ray-equations can be determined in a similar way as for the 1D-Helmholtz equation. In two dimensions general solutions become a summation of rays in directions θ with θ the angle of ray with respect to the x-axis increasing from the positive x-axis in counter-clockwise direction. This can then be written as:

$$u\left(x,y\right) = \int_0^{2\pi} a_\theta\left(x,y\right) e^{\iota\left(s_\theta\left(x,y\right)+\varphi_\theta\right)}\,\mathrm{d}\theta \tag{2.17}$$

with a_θ, s_θ, φ_θ functions of x and y for each specific ray direction θ. And as φ_θ is a constant this can be combined with s_θ. Therefore, for the 2D case, φ_θ can be chosen zero without loss of generality.

Substitution of the solution in the Helmholtz equation gives:

$$\frac{\partial^2}{\partial x^2}\int_0^{2\pi} a_\theta e^{\iota s_\theta}\,\mathrm{d}\theta + \frac{\partial^2}{\partial y^2}\int_0^{2\pi} a_\theta e^{\iota s_\theta}\,\mathrm{d}\theta + k\left(x,y\right)^2\int_0^{2\pi} a_\theta e^{\iota s_\theta}\,\mathrm{d}\theta = f\left(x,y\right) \tag{2.18}$$

As x and y are independent of θ the differential can be taken into the

integral leading to:

$$\int_0^{2\pi} \frac{\partial^2}{\partial x^2}\left[a_\theta e^{\iota s_\theta} + \frac{\partial^2}{\partial y^2} a_\theta e^{\iota s_\theta} + k\left(x,y\right)^2 a_\theta e^{\iota s_\theta}\right] \mathrm{d}\theta = \int_0^{2\pi} f_\theta\left(x,y\right) e^{\iota s_\theta}\, \mathrm{d}\theta \quad (2.19)$$

with:

$$\int_0^{2\pi} f_\theta\left(x,y\right) e^{\iota s_\theta}\, \mathrm{d}\theta = f\left(x,y\right) \quad (2.20)$$

Using the chain and product rule leads to:

$$\int_0^{2\pi} e^{\iota s_\theta}\left(\frac{\partial^2 a_\theta}{\partial x^2} + \frac{\partial^2 a_\theta}{\partial y^2} + \iota\left(\frac{\partial a_\theta \frac{\partial s_\theta}{\partial x}}{\partial x} + \frac{\partial a_\theta \frac{\partial s_\theta}{\partial y}}{\partial y}\right)\right) \mathrm{d}\theta + \int_0^{2\pi} e^{\iota s_\theta} \iota\left(\frac{\partial a_\theta}{\partial x}\frac{\partial s_\theta}{\partial x} + \frac{\partial a_\theta}{\partial y}\frac{\partial s_\theta}{\partial y}\right) \mathrm{d}\theta + \int_0^{2\pi} e^{\iota s_\theta}\left(k^2 - \left(\frac{\partial s_\theta}{\partial x}\right)^2 - \left(\frac{\partial s_\theta}{\partial y}\right)^2\right) a_\theta\, \mathrm{d}\theta = \int_0^{2\pi} f_\theta e^{\iota s_\theta}\, \mathrm{d}\theta \quad (2.21)$$

Both sides are integrals with respect to the same variable and with the same limits. Similar to the 1D case, this leads to an equation for all θ. The rays propagate in the θ-direction, therefore a rotated orthogonal coordinate system ξ, η, with ξ in the θ direction is preferable for each equation. The equation for direction θ then becomes:

$$\frac{\partial^2 a_\theta}{\partial \xi^2} + \frac{\partial^2 a_\theta}{\partial \eta^2} + \iota\left(\frac{\partial a_\theta \frac{\partial s_\theta}{\partial \xi}}{\partial \xi} + \frac{\partial a_\theta \frac{\partial s_\theta}{\partial \eta}}{\partial \eta} + \frac{\partial a_\theta}{\partial \xi}\frac{\partial s_\theta}{\partial \xi} + \frac{\partial a_\theta}{\partial \eta}\frac{\partial s_\theta}{\partial \eta}\right) + a_\theta\left(k^2 - \left(\frac{\partial s_\theta}{\partial \xi}\right)^2 - \left(\frac{\partial s_\theta}{\partial \eta}\right)^2\right) = f_\theta \quad (2.22)$$

Now the local behaviour of the solution around point Ξ, H is given by:

$$u_\theta\left(\xi,\eta\right) = a_\theta\left(\Xi,H\right) e^{\iota\left(k(\Xi,H)(\xi-\Xi)+\varphi_\theta(\Xi,H)\right)} \quad (2.23)$$

And in the same line of thought as the 1D case:

$$u_\theta\left(\Xi+\delta\xi,\eta\right) = a_\theta\left(\Xi+\delta\xi,\eta\right) e^{\iota k(\Xi,\eta)(\delta\xi)+\varphi_\theta(\Xi+\delta\xi,\eta)} \quad (2.24)$$

It will now be assumed that the total phase of a line Ξ can only be influenced by the wave-number, thus:

$$\int_{H}^{H+\delta\eta} \varphi_\theta\left(\Xi,\eta\right)\ \mathrm{d}\eta = \int_{H}^{H+\delta\eta} \varphi_\theta\left(\Xi+\delta\xi,\eta\right)\ \mathrm{d}\eta \tag{2.25}$$

And, again in the same line of thought as the 1D case, s_θ will now be introduced:

$$s_\theta\left(\Xi,\eta\right) = \varphi_\theta\left(\Xi,\eta\right) \tag{2.26a}$$

$$s_\theta\left(\Xi+\delta\xi,\eta\right) = k\left(\Xi,\eta\right)\delta\xi + \varphi_\theta\left(\Xi+\delta\xi,\eta\right) \tag{2.26b}$$

Therefore, using equations 2.25, 2.26a and 2.26b, $s_\theta\left(\xi,\eta\right)$ needs to satisfy:

$$\begin{aligned}&\lim_{\delta\xi\to 0,\delta\eta\to 0} \int_{\eta}^{\eta+\delta\eta} s_\theta\left(\xi+\delta\xi,\eta'\right)\ \mathrm{d}\eta' \\ &\quad= \lim_{\delta\xi\to 0,\delta\eta\to 0} \left(\delta\xi \int_{\eta}^{\eta+\delta\eta} k\left(\xi,\eta'\right)\ \mathrm{d}\eta' + \int_{\eta}^{\eta+\delta\eta} s_\theta\left(\xi,\eta'\right)\ \mathrm{d}\eta' \right)\end{aligned} \tag{2.27}$$

For constant k, and constant $s_\theta\left(0,\eta\right)$ the derivative with respect to η of s_θ will be zero for all ξ, while the derivative with respect to ξ of s_θ will be k. The equation will then change to:

$$\frac{\partial^2 a_\theta}{\partial\xi^2} + \frac{\partial^2 a_\theta}{\partial\eta^2} + 2\imath k\frac{\partial a_\theta}{\partial\xi} = f_\theta \tag{2.28}$$

And for this situation the homogeneous Helmholtz equation with a constant A_θ as boundary condition becomes:

$$u\left(x,y\right) = \int_{0}^{2\pi} A_\theta e^{\imath\left(k_{1\theta}x+k_{2\theta}y+\varphi_\theta\right)}\,\mathrm{d}\theta \tag{2.29}$$

with $k_{1\theta}^2 + k_{2\theta}^2 = k^2$, with $k_{1\theta} = k\cos\theta$ and $k_{2\theta} = k\sin\theta$.

Another solution for s_θ for the case of variable wave-number, that satisfies, with some assumptions, the conditions for the local behaviour is the solution of the eikonal equation:

$$\frac{\partial^2 s_\theta}{\partial\xi^2} + \frac{\partial^2 s_\theta}{\partial\eta^2} - k^2 = 0 \tag{2.30}$$

This equation has the advantage that it removes the last term of the left hand side in equation 2.22. It requires some assumptions however and at the moment the focus will be on the non-homogeneous equations with constant wave-number for the 2D case. Note that for the 1D case, the wave-number will be assumed to be variable, and a constant wave-number will only be used to compare analytic and numeric solutions.

The ray equations, which were derived in this chapter, will later be used, but the Helmholtz equation remains the equation to be solved. Analytical solutions can be derived for generic cases of the Helmholtz equation. Such a case is the 1D equation with Dirichlet boundary conditions, a constant k and simple or no forcing. A simple forcing is a non-zero f in a limited amount of points while f is zero in the remaining of the domain. For non-constant k and a complex forcing, analytical solutions are much more difficult or impossible to obtain. Therefore a numerical approach is required to solve the equations. The next chapter will show how the equations can be numerically approached.

Chapter 3

Numerical Solution

In the preceding chapter it has been shown that an analytic solution for complex cases is difficult or impossible to obtain. Therefore a numerical solution is required to approximate the exact solution of the problem. Several numerical methods are mentioned in section 1.2. The choice was made to use a Finite Difference Method to obtain a numerical solution.

3.1 Discretization

All numerical methods make use of some approximation of the equations of the mathematical model in discrete points, volumes, or elements in the domain, that leads to a system of algebraic equations. This approximation introduces errors with respect to the exact terms in the equations and therewith in the solution. To show the performance of a numerical method, the properties of this discretization can be studied for a case where the analytic solution is known.

In the finite difference methods combinations of Taylor series of the unknown functions are used to approximate the derivatives in the equations. For example, a second order accurate approximation to the Helmholtz equation on a uniform three dimensional mesh in a gridpoint $\left(x_i, y_j, z_k\right)$ is:

$$\frac{u^h_{i-1,j,k} - 2u^h_{i,j,k} + u^h_{i+1,j,k}}{\Delta x^2} + \frac{u^h_{i,j-1,k} - 2u^h_{i,j,k} + u^h_{i,j+1,k}}{\Delta y^2} + \frac{u^h_{i,j,k-1} - 2u^h_{i,j,k} + u^h_{i,j,k+1}}{\Delta z^2} + {k^h_{i,j,k}}^2 u^h_{i,j,k} = f^h_{i,j,k} \quad (3.1)$$

with Δx, Δy and Δz the mesh size in respectively x, y and z direction. Where $u^h_{i,j,k}$ is a representation of the unknown u, and where $k^h_{i,j,k}$ and $f^h_{i,j,k}$ are representations of k and f in the discrete points. If the functions are smooth one can simply take the value, e.g. $k\left(x_i, y_j, z_k\right)$. For non-smooth functions average values, for instance, of k and the f in the box of $\Delta x \times \Delta y \times \Delta z$ around the

discrete point are used. To reduce the amount of writing the operator acting on $u^h_{i,j,k}$ is referred to as $L^h \left\langle u^h \right\rangle_{i,j,k}$, thus:

$$L^h \left\langle u^h \right\rangle_{i,j,k} = f^h_{i,j,k} \tag{3.2}$$

Equation 3.1 for each point i, j, k leads to a system of algebraic equations that can be solved in two ways, direct or iteratively. For a system of linear equations a direct method is simply some sort of matrix inversion. Direct algorithms are very efficient for systems that have a small bandwidth, or that can easily be rewritten as such a system. However, for system of equations resulting from PDE problems, this bandwidth is usually equal to $\mathcal{O}\left(N^{D-1}\right)$, with D equals 1,2 or 3 for 1D, 2D and 3D problems, respectively. Therefore, for problems in 2D and 3D, these methods are relatively expensive. The alternative is to use an iterative method. A particular class of iterative methods are local processes, step by step changing the value of the unknown in a point, using the equation at that point and the values of the unknowns of the neighbouring points.

3.2 Iterative methods

3.2.1 Basic iterative techniques

Iterative methods correct a given approximation to the exact solution to compute a better approximation to this solution. This process is repeated until a desired accuracy is obtained. A correction of the given approximation is performed with a normalized difference between the right hand side, $f^h_{i,j,k}$, and the left hand side, $L \left\langle u^h \right\rangle_{i,j,k}$, of the equation, referred to as the residual. Simultaneous displacement methods use the given approximation for all points, whereas successive displacement methods use previously corrected values when treating the next equations. An example of a simultaneous displacement method is Jacobi relaxation. An example of a successive displacement method is Gauß-Seidel relaxation.

The choice for using a method depends among others on stability, data capacity and convergence speed. Simultaneous methods generally require more memory storage space than successive methods, as both the new and old approximation need to be stored. Another consideration is the suitability to parallelize the method. Successive displacement methods require special attention for a parallel computation, as the set of equations needs to be split, the method cannot be fully successive. For instance, Red-Black Gauß-Seidel relaxation makes use of a staggered sweep on a chessboard like grid. First the red points are relaxed in a sweep, and then the black points are relaxed.

All one point methods are based on correcting a given approximation to obtain a new approximation to the exact discrete solution. For a one point method in a 3D case this can be expressed as:

$$\hat{u}^h_{i,j,k} = \tilde{u}^h_{i,j,k} + \omega \delta^h_{i,j,k} \tag{3.3}$$

with:

$$\delta^h_{i,j,k} = \left(\left. \frac{\partial L \left\langle u^h \right\rangle_{i,j,k}}{\partial u^h_{i,j,k}} \right|_{\tilde{u}^h} \right)^{-1} \left(f^h_{i,j,k} - L^h \left\langle \bar{u}^h \right\rangle_{i,j,k} \right) \tag{3.4}$$

with $\bar{u}^h_{i,j,k} = \hat{u}^h_{i,j,k}$ when updated values of the new approximation will be used, and with $\bar{u}^h_{i,j,k} = \tilde{u}^h_{i,j,k}$ where values of the given approximation will be used. The relaxation factor ω can be used to perform under- or over-relaxation. For linear equations with $\omega = 1$ the value of $\tilde{u}^h_{i,j,k}$ itself does not influence $\hat{u}^h_{i,j,k}$ due to the normalization by the derivative to $\tilde{u}^h_{i,j,k}$ of the operator.

The error of a given approximation with respect to the exact discrete solution is given by:

$$\tilde{v}_{i,j,k} = u^h_{i,j,k} - \tilde{u}^h_{i,j,k} \tag{3.5}$$

As the exact discrete solution is generally not known the error has to be approximated. The residual is a measure for the error and is written as:

$$r_{i,j,k} = f^h_{i,j,k} - L \left\langle \bar{u}^h \right\rangle_{i,j,k} \tag{3.6}$$

where $r_{i,j,k} = 0$ if $\bar{u}^h_{i,j,k} = u^h_{i,j,k}$. Methods resulting, for simple cases, in a small error with respect to the exact analytic solution are unreliable if the residual does not approach machine accuracy.

3.2.2 Local Mode Analysis

The performance of iterative processes can be measured in terms of the reduction rate of the residual during each step of the process. An eigenvalue analysis, neglecting the effect of the boundary conditions, can be used to determine stability and convergence properties. A so called Local Mode Analysis(LMA) makes use of a Fourier series approximation of the error:

$$\tilde{v}^h_{i,j,k} = \sum_{0<|\theta_1|\leq\pi} \sum_{0<|\theta_2|\leq\pi} \sum_{0<|\theta_3|\leq\pi} \tilde{A}\left(\theta_1, \theta_2, \theta_3\right) e^{\iota\left(\theta_1 i + \theta_2 j + \theta_3 k\right)} \tag{3.7}$$

where θ_1, θ_2 and θ_3 are the frequency components in the x, y and z direction, respectively. $\tilde{A}\left(\theta_1, \theta_2, \theta_3\right)$ is the amplitude of the specific Fourier component of the given approximation.

The error after the relaxation is written in the same way, and is therefore written as:

$$\hat{v}^h_{i,j,k} = \sum_{0<|\theta_1|\leq\pi} \sum_{0<|\theta_2|\leq\pi} \sum_{0<|\theta_3|\leq\pi} \hat{A}\left(\theta_1, \theta_2, \theta_3\right) e^{\iota\left(\theta_1 i + \theta_2 j + \theta_3 k\right)} \tag{3.8}$$

Substitution equation 3.5 in equation 3.3 gives:

$$\hat{v}^h_{i,j,k} = \tilde{v}^h_{i,j,k} + \omega \left(\frac{\partial L \left\langle u^h \right\rangle_{i,j,k}}{\partial u^h} \bigg|_{\tilde{u}^h_{i,j,k}} \right)^{-1} \left(f^h_{i,j,k} - L^h \left\langle u^h - v^h \right\rangle_{i,j,k} \bigg|_{v^h = \bar{v}^h} \right) \quad (3.9)$$

with $\bar{v}^h_{i,j,k} = \hat{v}^h_{i,j,k}$ for all indices with values of the new approximation, and $\bar{v}^h_{i,j,k} = \tilde{v}^h_{i,j,k}$ for all indices with values of the current approximation. If the operator $L^h \langle\rangle$ is linear, as is the case for the Helmholtz equation, the solution and the error can be separated. This leads to elimination of u^h and f^h from equation 3.9 and a relation between only the error before and after relaxation. This gives:

$$\hat{v}^h_{i,j,k} = \tilde{v}^h_{i,j,k} - \omega \left(\frac{\partial L \left\langle u^h \right\rangle_{i,j,k}}{\partial u^h} \bigg|_{\tilde{u}^h_{i,j,k}} \right)^{-1} L^h \left\langle v^h \right\rangle_{i,j,k} \bigg|_{v^h = \bar{v}^h} \quad (3.10)$$

Substituting the Fourier series for the errors in this equation then makes it possible to determine the error amplification factor:

$$\mu\left(\theta_1, \theta_2, \theta_3\right) = \left| \frac{\hat{A}\left(\theta_1, \theta_2, \theta_3\right)}{\tilde{A}\left(\theta_1, \theta_2, \theta_3\right)} \right| \quad (3.11)$$

i.e. the new error divided by the current error for each Fourier component.

Convergence of the iterative method requires $\mu < 1$ for all Fourier frequency components $\mathcal{O}(h) < |\theta| \leq \pi$, with h the mesh size in the corresponding direction. The asymptotic convergence speed of an iterative scheme can then be determined by $\max(\mu)$ for $\mathcal{O}(h) \leq |\theta| \leq \pi$. Generally the asymptotic convergence speed is determined by the $\mathcal{O}(h)$ component and is of order $\bar{\mu} = \mathcal{O}(h^s)$, with $s = 2$ for Gauß-Seidel and Jacobi type of processes, this is shown in Appendix A.2. This implies that such processes are incapable of reducing low frequency error components efficiently, and therefore the required number of iterations increases significantly with decreasing mesh size.

3.2.3 Relaxation Schemes

Gauß-Seidel relaxation is a successive displacement method that will be analysed first. In Appendix A.2 a detailed description of its application to the discretized Helmholtz equation is given, as well as the results of a Local Mode Analysis. For the 1D problem the new values $\hat{u}^h_i$ are computed using the given values $\tilde{u}^h_i$, calculated in the previous sweep, according to:

$$\hat{u}^h_i = \tilde{u}^h_i + \frac{\omega \Delta x^2}{p^h_i} \left(f^h_i - \frac{\hat{u}^h_{i-1} + p^h_i \tilde{u}^h_i + \tilde{u}^h_{i+1}}{\Delta x^2} \right) \quad (3.12)$$

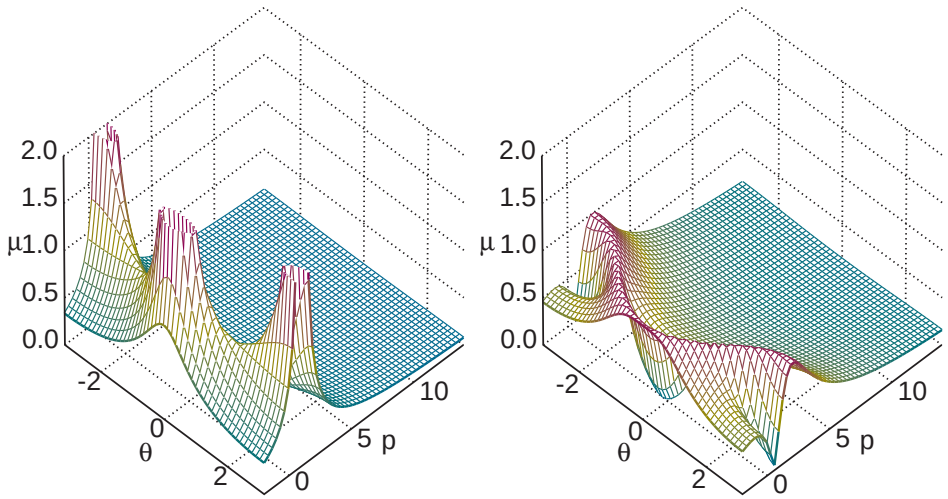

Figure 3.1: LMA for Gauß-Seidel(left) and Kaczmarz(right)

with $p_i^h = \left(k_i^h \Delta x\right)^2 - 2$. The error reduction factor for $\omega = 1$ then becomes:

$$\mu\left(\theta, p_i^h\right) = \frac{1}{\left|p_i^h + e^{-\iota\theta}\right|} \tag{3.13}$$

Generally μ only depends on the frequency of the component. For the Helmholtz equation however the term with $k^2 u$ introduces a dependency on the wave number. The graph of $\mu\left(\theta, p\right)$ for Gauß-Seidel relaxation in figure 3.1 shows this dependency. For $p \gg 0$ the error amplification factor is very small, making Gauß-Seidel relaxation very efficient. However, results with corresponding $k\Delta x$ lack any accuracy to represent solutions of the Helmholtz equation. For $p = -2$, the Poisson problem, the amplification factor does not exceed $\mu = 1$ and the method is stable. For $-2 < p < \sqrt{2}$, the amplification factor exceeds $\mu = 1$, resulting in an unstable scheme. These maxima are a result of the denominator of equation 3.13 going to zero at $\left(p = 1, \theta = \pm\pi\right)$ and at $\left(p = -1, \theta = 0\right)$. Therefore the overall behaviour of the relaxation process will be to diverge for these values of p.

An alternative relaxation process, that satiesfies the stability requirements, is the Kaczmarz relaxation. Kaczmarz relaxation is actually Gauß-Seidel relaxation applied to a transformed system of equations. The system to be solved, $\mathbf{A} \cdot \mathbf{u}^h = \mathbf{f}^h$, is now written as:

$$\left(\mathbf{A} \cdot \mathbf{A}^T\right) \cdot \mathbf{y}^h = \mathbf{f}^h \tag{3.14}$$

with:

$$\mathbf{u}^h = \mathbf{A}^T \cdot \mathbf{y}^h \tag{3.15}$$

In Appendix B a detailed description is given of its application to the discretized Helmholtz equation, as well as the results of a Local Mode Analysis. In the relaxation process grid points are scanned one by one and the values of $\tilde{u}^h$ in the point itself and its neighbours will be changed. For the 1D-problem the new and partly new values $\hat{\tilde{u}}_i^h$, $\tilde{\hat{u}}_i^h$ and $\hat{\tilde{u}}_i^h$ are computed, using the old values $\tilde{\tilde{u}}_i^h$, according to:

$$\begin{aligned} \hat{\tilde{u}}_{i-1}^h &= \tilde{\tilde{u}}_{i-1}^h + \delta_i^h \\ \tilde{\hat{u}}_i^h &= \tilde{\tilde{u}}_i^h + p_i^h \delta_i^h \ , \qquad i = 2, \ldots, n-2 \\ \hat{\tilde{u}}_{i+1}^h &= \tilde{\tilde{u}}_{i+1}^h + \delta_i^h \end{aligned} \tag{3.16}$$

with:

$$\delta_i^h = \omega \Delta x^2 \frac{\tilde{r}_i^h}{{p_i^h}^2 + 2} \tag{3.17}$$

A Local Mode Analysis, for constant k and $\omega = 1$, then gives:

$$\mu\left(\theta, p\right) = \frac{\left|2p + e^{\iota\theta}\right|}{\left|e^{-2\iota\theta} + 2pe^{-\iota\theta} + p^2 + 2\right|} \tag{3.18}$$

The graph of $\mu\left(\theta, p\right)$ is shown in figure 3.1. It can be observed that the maximum in this case does not exceed $\mu = 1$ and the process is therefore stable, although $\mu\left(\theta, p\right)$ is still close to $\mu = 1$ for components with $\cos\left(\theta\right) \approx -\frac{p}{2}$. For large p, Kaczmarz relaxation also has a very low $\bar{\mu}$, although Gauß-Seidel has a lower $\bar{\mu}$. For $p = -2$, the asymptotic convergence rate is $1 - \mathcal{O}\left(h^4\right)$ which is worse than for Gauß-Seidel, i.e. smooth components converge even more slowly. However, to be sure that the solver remains stable it is recommended to use Kaczmarz relaxation even if p is very near to -2.

A Local Mode Analysis for the discretized 2D-Helmholtz equation is not essentially different. The results show that Gauß-Seidel is unstable for low kh and fast for high kh, while Kaczmarz is stable for all kh, but slightly slower for high kh. Moreover there are combinations of two frequency components that have to be reduced. As an example, the Local Mode Analysis for 2D Gauß-Seidel results in:

$$\mu\left(\theta_1, \theta_2, k, \Delta x, \Delta y\right) = \frac{\left|(1-\omega)\left(k^2 - \frac{2}{\Delta x^2} - \frac{2}{\Delta y^2}\right) - \omega\left(\frac{e^{\iota\theta_1}}{\Delta x^2} + \frac{e^{\iota\theta_2}}{\Delta y^2}\right)\right|}{\left|k^2 - \frac{2}{\Delta x^2} - \frac{2}{\Delta y^2} + \omega\left(\frac{e^{-\iota\theta_1}}{\Delta x^2} + \frac{e^{-\iota\theta_2}}{\Delta y^2}\right)\right|} \tag{3.19}$$

In equation 3.19 μ is not only dependant on the frequency components θ_1, and θ_2, but also on k, Δx and Δy. This makes it preferable to use grids for which $\Delta x \approx \Delta y$.

3.3 Multi-Level method

In the last decades Multi-Level techniques have been developed for iteratively solving systems of algebraic equations, resulting from discretization of different types of differential and integral equations. Multi-Level methods are also called Multi-Grid methods or other similar names. Most of these methods make use of coarser grids as the target grid, to accelerate convergence, and moreover to reduce the calculation time needed to get converged results with the desired accuracy. To explain the principle of the technique the Poisson equation is often used. This equation is equal to the Helmholtz equation for $k = 0$.

In figure 3.1 it can be observed that for $k\Delta x$ at and near zero the maximum of the graph is at $\theta = 0$. This means that low frequency error components in the residual are not reduced efficiently. High frequency components on the other hand are very efficiently reduced, independent of the mesh size if $k = 0$. This also means that after a few relaxation sweeps the error is relatively smooth, and can therefore be described accurately on a coarser grid. This is the basic idea behind Multi-Level methods; a coarser scale is used to accelerate the error reduction on a fine scale.

The Multi-Level scheme performs a correction on the fine grid:

$$\hat{u}^h_{i,j,k} = \tilde{u}^h_{i,j,k} + \tilde{v}^h_{i,j,k} \tag{3.20}$$

Here an approximation to $\tilde{v}^h_{i,j,k}$ is obtained on a coarse grid, from a restricted set of equations:

$$L^H \left\langle u^H_{I,J,K} \right\rangle^H = f^H_{I,J,K} \tag{3.21}$$

The coarse grid variables $u^H_{I,J,K}$ and $f^H_{I,J,K}$ are not direct representations of $u^h_{i,j,k}$ and $f^h_{i,j,k}$. There are different representations possible for the fine grid error on the coarse grid. For a linear problem, with unchanging boundary conditions, the coarse grid variable $u^H_{I,J,K}$ is simply the representation of $\tilde{v}^h_{i,j,k}$ and $f^H_{I,J,K}$ the restricted fine grid residuals:

$$L^H \left\langle u^H_{I,J,K} \right\rangle = I^H_h \left\langle f^h_{i,j,k} - L^h \left\langle u^h_{i,j,k} \right\rangle \right\rangle \tag{3.22}$$

This is called the Correction Scheme (CR). $I^H_h \langle\rangle$ is an operator to restrict the fine grid residuals to the coarse grid in such a way that the smooth error components will be well represented and high frequent components, which cause an aliasing error, are filtered out. For the case of Dirichlet Boundary Conditions in the Correction Sceme the boundary conditions on the coarse grid will be zero.

The variable u^H is the coarse grid representation of the fine grid error and with a proper interpolation operator $I^h_H \langle\rangle$ this coarse grid solution can be used to perform a correction on the fine grid:

$$\hat{u}^h_{i,j,k} = \tilde{u}^h_{i,j,k} + I^h_H \left\langle u^H_{I,J,K} \right\rangle \tag{3.23}$$

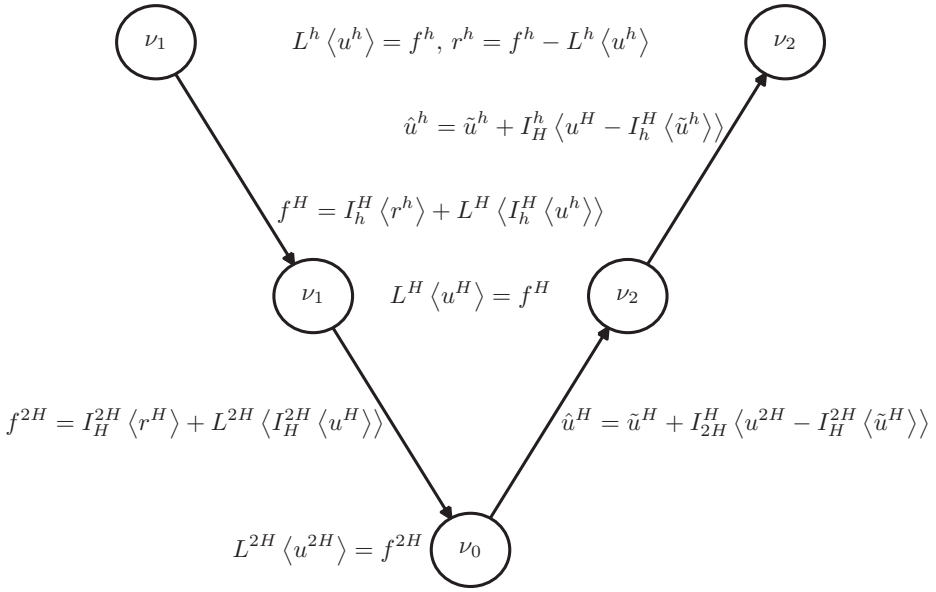

Figure 3.2: A three level Multi-Level cycle

It can be observed that when the residual on the fine grid is zero, the coarse grid equations will have zero as the solution, which is desired for a stationary process.

When the equations are non-linear or if coarse grid solutions influence the boundary conditions the function itself needs to be represented on the coarse grid too. The error will then be approximated by subtracting the interpolated fine grid solution from the coarse grid solution. This approach is called the Full Approximation Scheme (FAS) and the system of equations for this method changes to:

$$L^H \left\langle u^H_{I,J,K} \right\rangle = I_h^H \left\langle f^h_{i,j,k} - L^h \left\langle \tilde{u}^h_{i,j,k} \right\rangle \right\rangle + L^H \left\langle I_h^H \left\langle \tilde{u}^h_{i,j,k} \right\rangle \right\rangle \tag{3.24}$$

with the correction written as:

$$\hat{u}^h_{i,j,k} = \tilde{u}^h_{i,j,k} + I_H^h \left\langle u^H_{I,J,K} - I_h^H \left\langle \tilde{u}^h_{i,j,k} \right\rangle \right\rangle \tag{3.25}$$

Using FAS, a zero residual on the fine grid will result in no corrections, as $L^H \left\langle u^H_{I,J,K} \right\rangle = L^H \left\langle I_h^H \left\langle \tilde{u}^h_{i,j,k} \right\rangle \right\rangle$ will lead to $u^H_{I,J,K} = I_h^H \left\langle \tilde{u}^h_{i,j,k} \right\rangle$, and therefore $\hat{u}^h_{i,j,k} = \tilde{u}^h_{i,j,k}$. To solve equation 3.21 the same iterative procedure can be used as for solving the equations on the fine grid.

However, the coarser grid can still be relatively fine. Therefore the asymptotic convergence rate will still be slow. For equation 3.21 smooth error components can then be approximated on a coarser grid. That grid could require an even coarser grid until a grid is reached, for which further coarsening is less

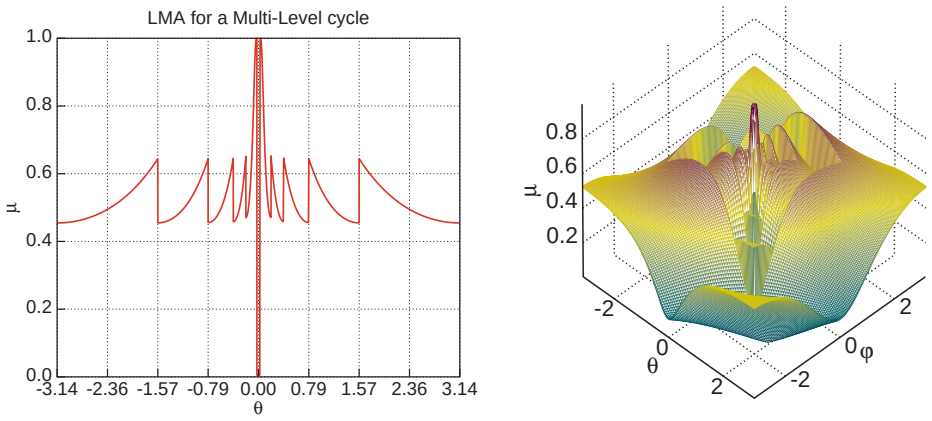

Figure 3.3: Local Mode Analysis for 1D(left) and 2D(right) with $k\Delta x = \frac{1}{32}$

efficient than calculation of the solution on that grid. The process of going to coarser grids while doing some relaxations on each grid level and then going back to finer grids again while at each stage doing a number of relaxations to reduce interpolation errors is called a coarse grid correction cycle. As an example, a graphical representation of a three level cycle is shown in figure 3.2.

For some equations it is possible to start the calculation on a coarse grid and use the interpolated coarse grid solution as a first estimate for the solution on a finer grid. This leads to the so called Full Multi-Grid(FMG) algorithm. For the Helmholtz equation this is not useful as coarse grids cannot provide a proper estimate of the fine grid solution in the highly indefinite case. Therefore it is assumed that only cycles are used starting at the required finest level grid.

An easy, often sufficiently efficient, way of coarsening is by increasing the mesh size by a factor two in each dimension. However, for the discretized Helmholtz equation the solution on coarse grids may lead to large phase and amplitude errors. These grids have to be skipped when performing a Multi-Level cycle. From Van Emden [3] it can be concluded that grids with $0.9 < k\Delta x < 2.75$ have to be skipped. It has also been concluded that a grid with $k\Delta x \approx 4$ is the suitable coarsest grid for relaxation to act as an exact solver.

For an eight level cycle with on the finest level $0 \leq k\Delta x \leq \frac{1}{2^4}$ a Local Mode Analysis is performed and the result is shown in figure 3.3. Even in the Multi-Level scheme there remain peaks where $\mu = 1$. Higher resolution results show that, for all $k\Delta x$, $\mu = 1$ occurs. However for those locations the actual convergence rate can be derived by a Taylor series expansion around that point for $\theta = \mathcal{O}(\Delta x)$. And as Δx is relatively high for the lower levels the convergence speed is still good. Therefore an asymptotic convergence rate of 0.65 per relaxation should theoretically be possible when using the Multi-Level

cycle.

In figure 3.3 the Local Mode Analysis for an eight level cycle with $k\Delta x = \frac{1}{32}$ is shown for the 2D-Helmholtz equation. It can be observed that μ is point symmetric around zero with a slight rotation with respect to the diagonals. It also follows that convergence in the diagonal directions is relatively slow for high frequency errors compared to high frequency errors in the horizontal and vertical directions.

3.4 Inter-grid operators

For the Multi-Level algorithm the discretized equations have to be restricted to the coarse grid and corrections have to be interpolated to the fine grid. Restriction operators have to reduce the influence of highly oscillatory components, but they also need to represent the smooth terms correctly. Interpolation operators need to represent a coarse grid function in a proper way on the fine grid. For interpolation of corrections a first order accurate interpolation is used. In other words errors are assumed to be linear between two grid points. In 1D the stencil of the interpolation is given by:

$$I_H^h = \frac{1}{2}\begin{bmatrix} 1 & 2 & 1 \end{bmatrix} \tag{3.26}$$

This means that an error at a coarse grid point will have a full contribution to a coinciding point on the fine grid and contributes with 50% to the direct neighbours. On the boundary the operator will be similar except that there is only one direct neighbour on the fine grid.

An operator for restriction follows from taking the transpose of the interpolation scheme multiplied with $\left(\frac{h}{H}\right)^d$. It is written as:

$$I_h^H = \frac{1}{4}\begin{bmatrix} 1 & 2 & 1 \end{bmatrix} \tag{3.27}$$

This is referred to as full weighting. Full weighting will be used for both the restriction of the right hand side and for the restriction of the fine grid solution. However, it is possible to use injection for the fine grid solution as is used by Van Emden [3]. Injection requires less calculation time, but it can be sensitive to aliasing errors. On the boundary the restriction used depends on the boundary conditions. For Dirichlet conditions implemented in the right hand side of the equation injection can be used.

For two and more dimensions, interpolation and restriction can be carried out one dimension at a time, using the 1D operators. For example the stencil of interpolation in 2D becomes:

$$I_H^h = \frac{1}{4}\begin{bmatrix} 1 & 2 & 1 \\ 2 & 4 & 2 \\ 1 & 2 & 1 \end{bmatrix} \tag{3.28}$$

And the stencil of restriction with full weighting becomes:

$$I_h^H = \frac{1}{16}\begin{bmatrix} 1 & 2 & 1 \\ 2 & 4 & 2 \\ 1 & 2 & 1 \end{bmatrix} \tag{3.29}$$

3.5 The Ray Cycle

In the preceding section it was shown that a Multi-Level scheme can drastically improve the performance of iterative solution schemes. However, when applied to the Helmholtz equation the standard Multi-Level coarse grid correction cycle, after initial good error reduction, shows a strong decrease in rate of convergence. The error components in the residual that remains, are components with the same frequency as that of the solution. These characteristic components are not seen by the operator and are therefore not reduced by the cycle.

The basis of the Multi-Level methodology is to approximate each error component in such a way and on a scale that it can be reduced efficiently. Smooth components can be efficiently reduced on a coarser grid, because they are relatively high frequent with respect to the mesh size of that grid. For the Helmholtz problem this implies that an additional type of cycle is required to efficiently reduce the characteristic components. This will be referred to as the Ray Cycle. The standard Multi-Level cycle will from now on be referred to as the Wave Cycle.

It has been shown in Chapter 2 that solutions of the Helmholtz equation can be written as a combination of rays in all directions. Therefore solutions of the discrete Helmholtz equation will also be a combination of rays, and each ray has to satisfy equation 2.22. However, it is impossible to solve this problem exact as an infinite number of equations will have to be solved. A discrete number of ray equations will have to be solved to represent all ray functions. An increase in the number of directions leads to smoother ray functions. Grids that can lead to efficient solution procedures for the ray equations are relatively coarse. On these coarse grids only a limited amount of rays is required to acquire smooth ray functions. Typically eight rays should be sufficient for the grids on which these problems will be solved, which is described by Livshits and Brandt[1].

For these eight rays the right hand side has to be determined to satisfy equation 2.20. On a coarse grid the right hand side is a function of the fine grid residual, and can be written as:

$$f_{I,J}^H = I_h^H \left(f_{i,j}^h - L \langle u \rangle_{i,j}^h \right) \tag{3.30}$$

The residual is a combination of the characteristic error components and

can therefore be written as:

$$r_{i,j}^h = \int_0^{2\pi} r_{\theta,i,j}^h e^{\iota\left(s_{\theta,i,j}+\varphi_\theta\right)} \,\mathrm{d}\theta \tag{3.31}$$

The right hand side f_θ^H is determined by r_θ^h. Thus for each of the rays the appropriate part of the residual needs to be separated from the complete residual. These characteristic error component amplitudes are therefore determined by a separation algorithm. Separation can efficiently be achieved on grids, for which $k\Delta x \approx 1$. The next chapter treats the separation algorithm in detail. For the general principle behind the Wave-Ray algorithm it is only important that such a separation is possible. As the right hand sides of the ray-equations can now be determined, these equations can be solved. Boundary conditions are imposed on the side from which the ray is radiating. On the separation grid, with $k\Delta x \approx 1$, the solutions of the ray-equations are then used to correct the wave solution:

$$\hat{u}_{i,j} = \tilde{u}_{i,j} + \sum_{n=0}^{7} \left(\hat{a}_{n\frac{\pi}{4},i,j}^h - \tilde{a}_{n\frac{\pi}{4},i,j}^h \right) e^{\iota\left(s_{n\frac{\pi}{4},i,j}+\varphi_{n\frac{\pi}{4}}\right)} \tag{3.32}$$

With $\tilde{a}_\theta^h$ the solution of the previous Ray Cycle.

Contrary to correction in a standard Multi-Level cycle with Dirichlet boundary conditions, a correction also has to be performed for the boundary points. This requires a Full Approximation Scheme for at least the Ray Cycle. It also requires the boundary conditions to be zero in the first Wave-Cycle. Using the correction scheme, the Radiation Boundary Conditions can be introduced in the wave solution using the ray solutions. The Dirichlet boundary conditions can in that way change each cycle until a converged solution is obtained. The changing Dirichlet Conditions not only introduce Radiation Boundary Conditions in the Helmholtz equation. They also adapt the conditions to arbitrary right hand sides, as the rays radiated from sources are taken into account by the ray equations.

3.6 The ray equations

To be able to implement the Ray Cycle, the ray equations need to be discretized. As the equations have a strong directional dependency, an upstream scheme is preferable. Using a first order upwind scheme for the first derivative and a second order central scheme for the second derivative, the discrete equations for the 1D rays are:

$$\frac{a_{i+1}^h - 2a_i^h + a_{i-1}^h}{\Delta x^2} + \iota \left(\frac{a_i^h k_i^h - a_{i-1}^h k_{i-1}^h}{\Delta x} + k_i^h \frac{a_i^h - a_{i-1}^h}{\Delta x} \right) = f_{a,i}^h \tag{3.33a}$$

$$\frac{b^h_{i+1} - 2b^h_i + b^h_{i-1}}{\Delta x^2} + \iota \left(\frac{b^h_i k^h_i - b^h_{i+1} k^h_{i+1}}{\Delta x} + k^h_i \frac{b^h_i - b^h_{i+1}}{\Delta x} \right) = f^h_{b,i} \qquad (3.33b)$$

The advantage of equations 3.33 is that they can be solved very efficiently, using downstream marching in relaxation. However, even though the functions to be solved are smooth and are used for a coarse grid correction of the wave equations, a second order accurate scheme, with an upwind second order derivative, is preferred. This can be acquired using a staggered configuration. The equation is defined at the cell centres, using second order accurate discretizations for both the first and second order derivative. The equations, obtained using a staggered grid, are:

$$L^h \left\langle a^h \right\rangle_{i-\frac{1}{2}} = \frac{a^h_{i+1} - a^h_i - a^h_{i-1} - a^h_{i-2}}{2\Delta x^2} + \iota \left(\frac{a^h_i k^h_i - a^h_{i-1} k^h_{i-1}}{\Delta x} + k^h_{i-\frac{1}{2}} \frac{a^h_i - a^h_{i-1}}{\Delta x} \right) = f^h_{a,i-\frac{1}{2}} \qquad (3.34a)$$

$$L^h \left\langle b^h \right\rangle_{i+\frac{1}{2}} = \frac{b^h_{i+2} - b^h_{i+1} - b^h_i + b^h_{i-1}}{2\Delta x^2} + \iota \left(\frac{b^h_i k^h_i - b^h_{i+1} k^h_{i+1}}{\Delta x} + k^h_{i+\frac{1}{2}} \frac{b^h_i - b^h_{i+1}}{\Delta x} \right) = f^h_{b,i+\frac{1}{2}} \qquad (3.34b)$$

This staggered approach has the advantage that it has the same order of accuracy as is used in the discretization of the Helmholtz equation itself. However, it requires information of the residual and the wave-number in the cell centres instead of the grid points. Depending on the method of separation, this requires coarsening of the separated residual, with shifted weighting to the grid of the ray equations. Finally, as the wave-number is known in all points of the fine grid, the wave-number in the Ray grid midpoints can directly be obtained without additional complications.

Separation has to be performed on a level where the characteristic error components are smooth. This requires $k\Delta x \approx 1$ on the grid where separation and correction is performed. Grids on which the ray equation can be efficiently solved require $k\Delta x \approx 4$, see also Van Emden [3]. This implies that two coarsening steps with a factor two can be used in the process of separation of the residual to obtain the right hand sides of the ray equations.

For the 2D problem, the ray equations have a strong directional dependency in positive ξ-direction. Therefore, again, an upstream scheme is required. Similar to the 1D case methods can either use standard grids or staggered grids. A first order upstream scheme, with second order discretization for second

derivatives, for constant wave-number can be written as:

$$L^h \left\langle a^h \right\rangle_{i,j} = \frac{a^h_{i-1,j} - 2a^h_{i,j} + a^h_{i+1,j}}{\Delta\xi^2} + \frac{a^h_{i,j-1} - 2a^h_{i,j} + a^h_{i,j+1}}{\Delta\eta^2} + 2\imath k \frac{a^h_{i,j} - a^h_{i-1,j}}{\Delta\xi} = f^h_{i,j} \quad (3.35)$$

For non-constant wave-number, first order derivatives in η direction have to be discretized. This can be done with for example a central scheme:

$$\frac{\partial a}{\partial \eta} = \frac{a^h_{i,j+1} - a^h_{i,j-1}}{2\Delta\eta} + \mathcal{O}\left(\Delta\eta^2\right) \quad (3.36)$$

Furthermore, in the case that the wave-number is not constant, derivatives with respect to ξ and η for the phase function s are required in equation 2.22. These first order derivatives for s can be calculated once on the finest grid and stored for use in the Ray cycle, as they do not change during the solution process. On the fine grid these derivatives can be calculated with a central scheme. However, it is also possible to take upstream derivatives. This requires knowledge of the directional dependency, to determine the upstream direction in η-direction.

In a similar way as was the case for 1D, another option is to use a staggered approach. An example is the Crank-Nicolson scheme. The scheme combines an explicit and implicit scheme with equal weighting. It therefore uses derivatives in η-direction of the unknown current spatial step in ξ-direction and the known former spatial step in ξ-direction. It results in a second order accurate approximation for both the first and second order derivatives. This scheme is widely used in time dependent convection problems. For constant wave-number, the scheme can be written as:

$$L^h \left\langle a^h \right\rangle_{i-\frac{1}{2},j} = \frac{a^h_{i-2,j} - 2a^h_{i-1,j} + a^h_{i,j}}{\Delta\xi^2} + \frac{a^h_{i,j-1} - 2a^h_{i,j} + a^h_{i,j+1}}{2\Delta\eta^2} + \frac{a^h_{i-1,j-1} - 2a^h_{i-1,j} + a^h_{i-1,j+1}}{2\Delta\eta^2} + 2\imath k \frac{a^h_{i,j} - a^h_{i-1,j}}{\Delta\xi} = f^h_{i-\frac{1}{2},j} \quad (3.37)$$

For varying wave-number, the first order derivatives will be discretized as in equation 3.36. In a similar way as the second order derivatives in η direction, the derivative at $i-1$ and at i will both contribute similarly to the operator.

To implement the scheme, it is preferable to have $\Delta x = \Delta y = h$ for the wave solution. The grid on which separation can efficiently be performed requires $kh \approx 1$, similar to the 1D case. Grids on which the ray equations can be efficiently solved require $k\Delta\xi \approx 4$ and $k\Delta\eta \approx 2$, see also Livshits and Brandt [1]. This implies that during the process of separation of residuals the grids have to be coarsened twice in ξ-direction and once in η-direction.

3.7 Wave-Ray Multi-Level algorithm

In preceding sections the basic iterative methods, and the basics of the Wave and Ray Cycle were shown. These elements will now be combined into the Wave-Ray Multi-Level algorithm. For the chosen discretization of the Helmholtz equation, solutions on grids with too large a value of kh lead to large phase and amplitude errors. These coarse grids would give very bad corrections, and therefore they are excluded from the relaxation in the Wave Cycle. Also, different relaxation methods are used on different grids in view of stability. Finally the number of relaxations used, can either be chosen constant, or can be chosen variable to obtain equal asymptotic convergence rates on the different grids. By Van Emden[3] several possibilities were tested and limitations and parameters indicated.

In the Wave Cycle the number of relaxations before restriction will be $\nu_1 = 2$ on all grids that are not excluded. Grids with $1.1 < kh < 2.75$ will be excluded from relaxations, as solutions on these grids will lead to increased errors due to phase and amplitude errors. On grids with $kh \leq 2$ the Kaczmarz scheme will be used, as a Local Mode Analysis predicts unstable solutions with a Gauß-Seidel scheme. On coarser grids with $kh \geq 2.75$ the Gauß-Seidel scheme will be used, as on these grids the scheme predicts a better convergence rate. Moreover the Gauß-Seidel scheme is computationally less demanding than the Kaczmarz scheme, therefore it should be preferred even if predicted convergence rates are the same. On the coarsest wave grid, with $kh \approx 4$, $\nu_0 = 10$ relaxations will be performed. On grids with $kh > 0.25$ no relaxations will be performed after correction. On the other grids $\nu_2 = 1$ relaxations will be carried out. Finally, when the finest level has been reached, the Ray Cycle will be used, to solve the remaining characteristic error components, which are not properly reduced by the Wave Cycle.

In the first part of the Ray Cycle the fine grid equations will be restricted without any relaxations to a grid with $kh \approx 1$. On this grid the separation will be performed including restriction to the ray grids. On the ray grids the radiation boundary conditions will be introduced and the ray equations will be solved using Gauß-Seidel relaxation. The Ray solutions will then be interpolated to the grid for which separation was performed and will be used for correction of the wave solution. Finally, regular correction is performed up to the finest grid, and for grids with $kh \leq 0.75$ $\nu_3 = 1$ relaxation will be performed.

In figure 3.4 a schematic representation is given for the 1D case. The 2D scheme is much the same except that the restrictions from the separation grid to the ray grids is now included in the separation process. In the used solution method a specific number of relaxations is performed on each grid and a specific number of cycles is used. Alternatively, cycles and relaxation processes can be carried out automatically until a converged solution has been reached.

Basic inter-grid routines and grid specific routines have been shown in this Chapter. The target of the separation process is described and assuming a

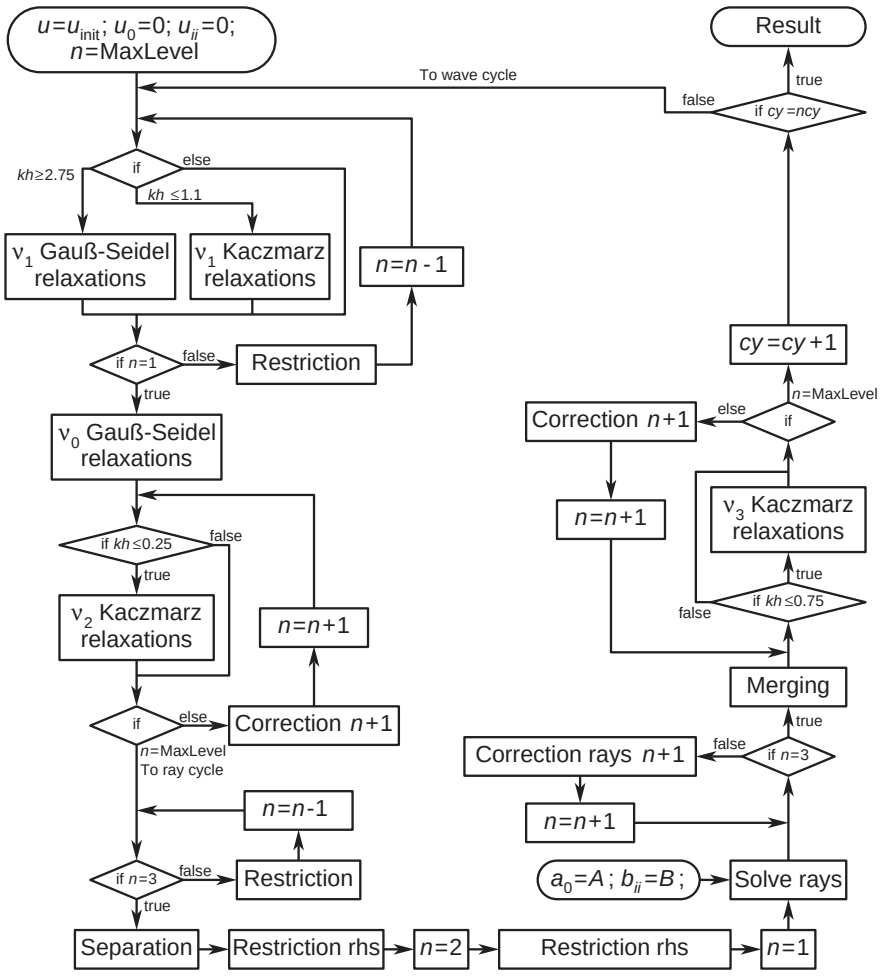

Figure 3.4: The Wave-Ray Multi-Level scheme for 1D

working separation, the Multi-Level scheme has been extended to a Wave-Ray scheme. Separation is essential for the Ray Cycle, the next chapter will treat this topic.

Chapter 4

Separation

In the previous chapter the Multi-Level Wave-Ray algorithm was described. Details of relaxation, restriction and interpolation were presented. In this chapter the separation process will be discussed. Note that separation does not refer to a separation of variables, for instance of time and spatial components, as was used in the derivation of the Helmholtz equation. In Chapter 2 it was shown that the right hand side can be written as a combination of rays in all directions. From a given right hand side the separation process determines the amplitudes of the different ray contributions. Below, first the 1D case will be presented. Subsequently, the more complicated 2D case is described.

4.1 Separation in one dimension

4.1.1 Separation scheme

Solutions of the Helmholtz equation for the 1D case are constructed from two rays: One ray representing a standing wave propagating from the left side of the domain and one representing a standing wave propagating from the right side of the domain, see also equation 2.2. Implemented in a Multi-Level cycle the right hand sides of the ray equations are:

$$f_a^H = S_{ah}^H \left\langle r^h \right\rangle + L^H \left\langle a_{old}^H \right\rangle \tag{4.1a}$$

$$f_b^H = S_{bh}^H \left\langle r^h \right\rangle + L^H \left\langle b_{old}^H \right\rangle \tag{4.1b}$$

With $S\langle\rangle$ an operator, or a series of operators, starting on the fine grid leading to the amplitude of the specific ray residual on the coarser ray grid.

Separation takes place on a grid with $k\Delta x \approx 1$ and the first step aims to render terms of the required ray almost constant through multiplication with the inverse of the particular ray function sought:

$$re^{-\iota\left(s(x)+\varphi_a\right)} = r_a + r_b e^{-2\iota\left(s(x)+\varphi_b+\varphi_a\right)} \tag{4.2a}$$

$$re^{\iota\left(s(x)+\varphi_b\right)} = r_b + r_a e^{2\iota\left(s(x)+\varphi_b+\varphi_a\right)} \tag{4.2b}$$

This operation not only makes the required term very smooth, but it also makes the other terms highly oscillatory with respect to the grid size. This part can now easily be removed by weighting to a grid twice as coarse. Next the residual will be coarsened, but now by a shifted full weighting, as the ray discretization is defined, and thus requires the residual, in the centre of a grid cell. Note that $k\Delta x \approx 1$ is required for efficient removal by weighting of these components. With shifted weighting all indices, both on the coarse and fine grid, are shifted with one with respect to the standard full weighting. This requires special attention near the boundaries, as the boundary points have a zero residual, by definition, because of the Dirichlet boundary conditions.

An alternative to standard full weighting with a $\frac{1}{4}\begin{bmatrix} 1 & 2 & 1 \end{bmatrix}$ scheme, is to use specific weights:

$$I_h^H \langle\rangle = \begin{bmatrix} w_1 & w_2 & w_3 \end{bmatrix} \tag{4.3}$$

And these weights are defined such that components of the required ray remain constant and the now highly oscillatory components of the other ray are removed completely:

$$w_1 e^{\iota 2k(x)\Delta x} + w_2 + w_3 e^{-\iota 2k(x)\Delta x} = 0 \tag{4.4a}$$

$$w_1 + w_2 + w_3 = 1 \tag{4.4b}$$

$$w_1 = w_3 \tag{4.4c}$$

Resulting in:

$$w_2 = 1 - 2w_1 = 1 - 2\frac{1}{2 - e^{2\iota k_i \Delta x} - e^{-2\iota k_i \Delta x}} \tag{4.5}$$

As the weighting is symmetric, equation 4.4c, this operator works for both the a- and b-ray. Equation 4.4b forces the weighting factors to satisfy the condition that constant terms remain constant. If this weighting is used, it is possible to use injection instead of full weighting from the intermediate grid to the ray grid. Calculation of the weighting factors however either costs more calculation time in the separation process or more memory to store the coefficients.

4.1.2 Separation results

To illustrate the performance of both separation methods, separation is applied to an example function of the form:

$$r = e^{\iota s(x)} + 2e^{-\iota s(x)} \tag{4.6}$$

with:

$$s(x) = \frac{\left(1 + \operatorname{sign}(x)\,0.1\right)\pi}{64} x + \frac{0.9\pi}{64}\pi \tag{4.7}$$

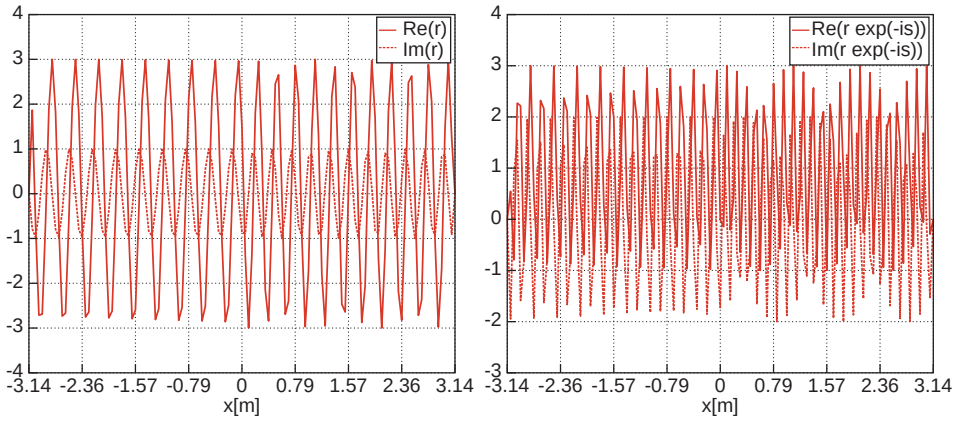

Figure 4.1: The test ray $e^{is(x)} + 2e^{-is(x)}$(left), and after multiplication with the inverse of ray a, $e^{-\imath s(x)}$(right)

In figure 4.1 this function is shown. Also shown in figure 4.1 is the resulting function after multiplication with $e^{-\imath s(x)}$. It can be observed that this leads to a result with oscillations with twice the frequency as before the multiplication, as should be to be able to perform separation by weighting.

In figure 4.2 the result of the application of both weighting methods are shown. Both types of weighting result in a smooth function. However, standard full weighting results in an oscillatory function, and is clearly less smooth in the region with an increasing slope of $s(x)$, with a higher wave-number. Standard weighting factors clearly cannot remove the undesired oscillations completely. Coarsening with pre-calculated weighting factors in the first coarsening step gives an almost smooth function in the entire domain and the result exhibits no noticeable oscillations any more.

To explain the difference in performance for standard weighting and the alternative method, the actual weighting factors obtained with the alternative method are needed. The weighting factors for $kh \approx 1$ are:

$$\mathbf{w} \approx \begin{bmatrix} 0.35 & 0.3 & 0.35 \end{bmatrix} \tag{4.8}$$

These factors differ a lot from the standard weighting factors. When kh gets larger, the weighting factors get closer to the standard weighting factors. This explains the better result for the part with a large wave-number after the first coarsening, relative to the part with a low wave-number. For the second coarsening however, the oscillatory components will have a frequency relative to the grid of $kh \approx 4$. For this step the standard weighting is closer to specific weights for low frequencies, and moves further away from those weights when the wave-number gets larger. This causes the better result for low wave-numbers than for high wave-numbers.

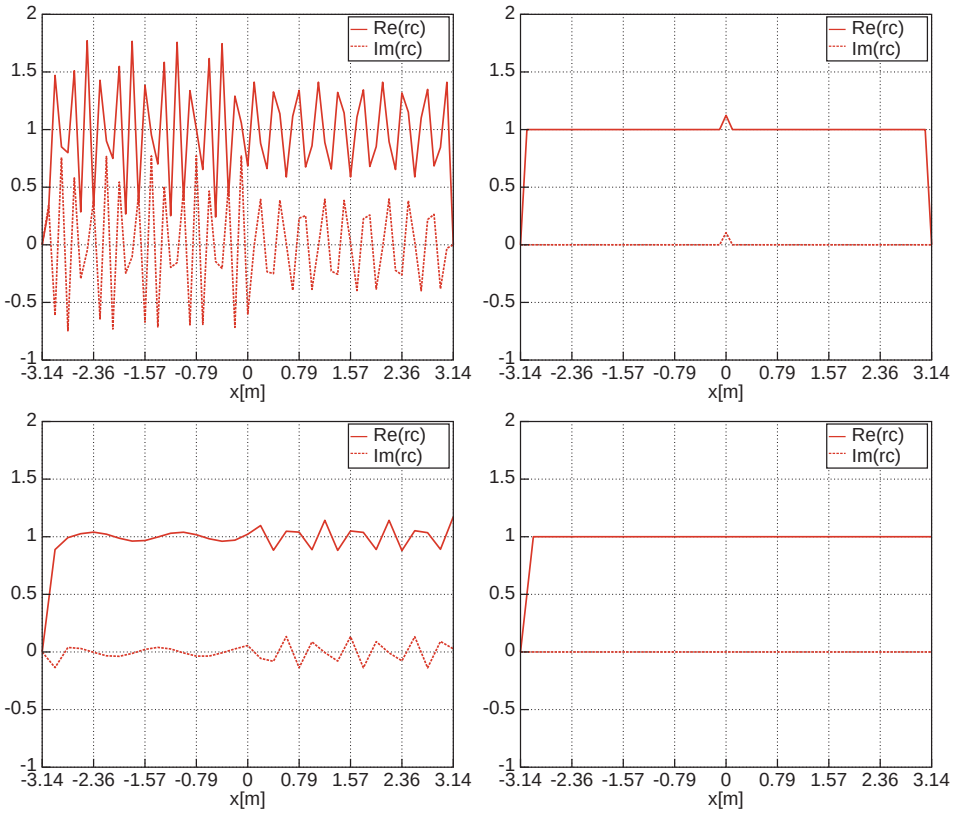

Figure 4.2: Coarsening using standard weighting factors(left), and calculated weighting factors(right), both after the first coarsening(above) and after the last coarsening(below)

The difference in performance of standard weights and specific weights is significant. This makes specific, calculated, weighs preferable, and this will therefore be used for the separation scheme.

4.2 Separation in two dimensional space

4.2.1 Separation scheme

Separation in the 2D space is based on the same principle as in the 1D space. Multiplying the residual by the inverse of the oscillatory part of the required component makes the component itself constant whereas the other components remain oscillatory. Weighting can then remove oscillations and a right hand side can be obtained representing the required component. Even though the principle is straightforward, in 2D its implementation is not straightforward. An infinite number of rays can occur instead of only two. These rays are represented using a discrete number of directions. This number should be sufficiently large to ensure that the ray functions themselves are sufficiently smooth on the scale at which they are solved.

In this case we assume, based on work by Livshits and Brandt [1], a fixed number of eight of these principal directions. The separation procedure for one ray will first be given and subsequently results for several directions will be shown.

A representation of the residual in terms of eight rays can be written as:

$$r = \sum_{n=0}^{n=7} r_n e^{\iota s_n(\xi_n,\eta_n)} \tag{4.9}$$

Where ξ_n is the principal direction of the ray in which s_n will locally increase with the wave-number. The principal directions are assumed to be uniformly distributed. In the case of eight directions they differ by an angle of $\frac{1}{4}\pi$ with respect to each other. As with separation in the 1D case, the first step will be to divide the residual by the required frequency. As an example ray direction 0, the positive x-direction, will be separated. The first step leads to:

$$re^{-\iota s_0(x,y)} = r_0 + \sum_{n=1}^{n=7} r_n e^{\iota(s_n(\xi_n,\eta_n)-s_0(x,y))} \tag{4.10}$$

In Chapter 2, s_n was defined in such a way that the local behaviour is $e^{\iota k\Delta\xi}$ and therefore a circle with principle directions ξ and with the Fourier component frequency $k\Delta\xi$ can be obtained as shown in figure 4.3. Multiplying the residual by the inverse of the required ray principal component leads to a shift of that ray to the origin, leading to a local behaviour for the remaining components in the residual $e^{\iota k(\Delta\xi_n-\Delta x)}$, as shown in the right of figure 4.3.

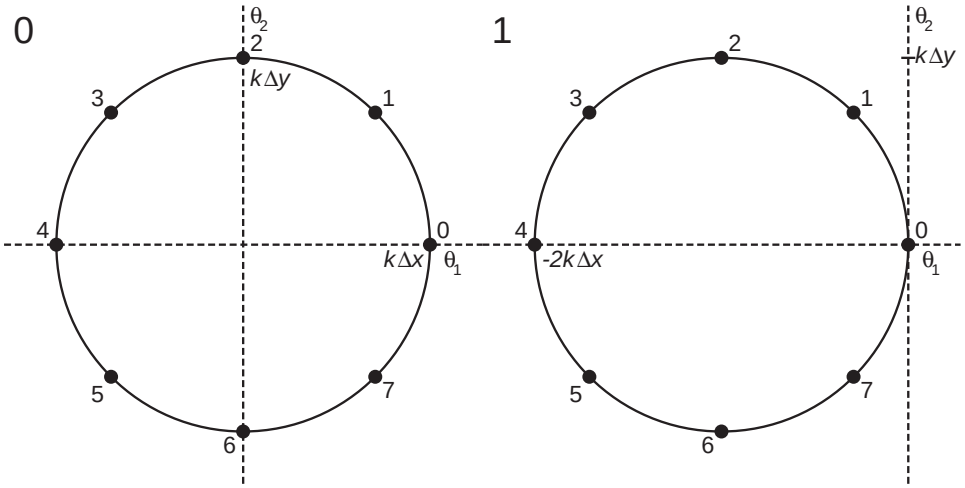

Figure 4.3: Circle with Fourier components of the principal components with radius $k\Delta\xi$ before(left) and after(right) multiplying by the inverse of the principal component of ray 0

The next task is to eliminate these remaining components. First, the opposite ray direction 4 will be eliminated. This component has now become highly oscillatory and can therefore be reduced efficiently on a grid with $kh \approx 1$ by a weighted coarsening process in x-direction. This is done similar to the 1D problem:

$$I_h^H \langle\rangle = \begin{bmatrix} w_1 & w_2 & w_3 \end{bmatrix} \tag{4.11}$$

with:

$$w_1 e^{2\imath k_{i,j}\Delta x} + w_2 + w_3 e^{-2\imath k_{i,j}\Delta x} = 0 \tag{4.12a}$$

$$w_1 + w_2 + w_3 = 1 \tag{4.12b}$$

$$w_1 = w_3 \tag{4.12c}$$

Resulting in:

$$w_2 = 1 - 2w_1 = 1 - 2\frac{1}{2 - e^{2\imath k_{i,j}\Delta x} - e^{-2\imath k_{i,j}\Delta x}} \tag{4.13}$$

And for $i = 2I$:

$$u_{I,j} = w_1 u_{i-1,j} + w_2 u_{i,j} + w_3 u_{i+1,j} \tag{4.14}$$

After this step, direction 4 will almost be removed from the remaining residual. Another result of the coarsening is that all remaining components become twice as high in frequency, with respect to the mesh size, in the x-direction as they previously were. The upper left of figure 4.4 shows this result. The circle has been stretched in x direction due to the coarsening and ray direction 4 has been shown with a dotted circle, as it is almost invisible in the resulting residual.

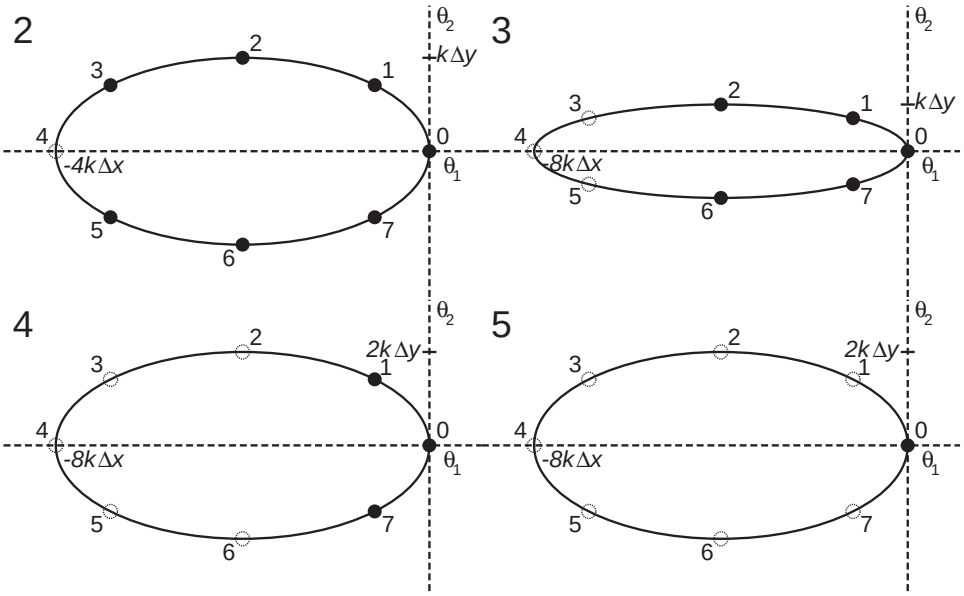

Figure 4.4: The stretched circle of the Fourier frequencies of the principle components with the eliminated frequencies after each weighting

Directions 3 and 5 are now at high frequency and will be removed by a second weighted coarsening in the x-direction. A set of equations similar to equations 4.12 results in:

$$w_2 = 1 - 2w_1 = 1 - 2\frac{1}{2 - e^{\iota k_{i,j}(2+\sqrt{2})\Delta x} - e^{-\iota k_{i,j}(2+\sqrt{2})\Delta x}} \tag{4.15}$$

And for i the index of the grid points on the grid after the first coarsening and $i = 2I$ this is again:

$$u_{I,j} = w_1 u_{i-1,j} + w_2 u_{i,j} + w_3 u_{i+1,j} \tag{4.16}$$

The frequency circle is again stretched in the x-direction. Ray-directions 3 to 5 are now, almost, removed. This can be seen in the upper right of figure 4.4. Following the lines of thought of Livshits and Brandt [1] the x-direction has a coarseness required for the Ray-grid. The y-direction is not yet as coarse as required, therefore the next weighted coarsening will be in that direction. This step aims to eliminate ray-directions 2 and 6. Again using a set of equations similar to equations 4.12 results in:

$$w_2 = 1 - 2w_1 = 1 - 2\frac{1}{2 - e^{\iota k_{i,j}\Delta y} - e^{-\iota k_{i,j}\Delta y}} \tag{4.17}$$

And for I the index of the grid points on the ray-grid and $j = 2J$ this is again:

$$u_{I,J} = w_1 u_{I,j-1} + w_2 u_{I,j} + w_3 u_{I,j+1} \tag{4.18}$$

As weighting is symmetric this weighting will remove both ray-directions 2 and 6. The frequency circle will now be stretched in y direction, and ray-directions 2 to 6 are almost removed. This is shown in the lower left of figure 4.4. The current grid has the required coarseness of the ray-grid. The last step will therefore be a weighting in one of the directions without coarsening. An asymmetric weighting is required at the boundaries, because no coarsening takes place and the boundary is not part of the residual with principal components. The remaining directions 1 and 7 have different components in the y-direction. The components associated with the x-direction however are the same, and asymmetric weighting in that direction will therefore still remove both ray-directions.

The equations for the inner region of the domain are still similar as equations 4.12, resulting in:

$$w_2 = 1 - 2w_1 = 1 - 2\frac{1}{2 - e^{\iota k_{i,j}(4-2\sqrt{2})\Delta x} - e^{-\iota k_{i,j}(4-2\sqrt{2})\Delta x}} \tag{4.19}$$

Used in:

$$u_{I,J} = w_1 u_{I-1,J} + w_2 u_{I,J} + w_3 u_{I+1,J} \tag{4.20}$$

For the left boundary the weighting equations change to:

$$w_2 + w_3 e^{-(4-2\sqrt{2})\iota k_{i,j}\Delta x} = 0 \tag{4.21a}$$

$$w_2 + w_3 = 1 \tag{4.21b}$$

Resulting in:

$$w_2 = 1 - w_3 = 1 - \frac{1}{1 - e^{-\iota k_{i,j}(4-2\sqrt{2})\Delta x}} \tag{4.22}$$

And used for:

$$u_{1,J} = w_2 u_{1,J} + w_3 u_{2,J} \tag{4.23}$$

For the right boundary the weighting equations change to:

$$w_1 e^{(4-2\sqrt{2})\iota k_{i,j}\Delta x} + w_2 = 0 \tag{4.24a}$$

$$w_1 + w_2 = 1 \tag{4.24b}$$

Resulting in:

$$w_2 = 1 - w_3 = 1 - \frac{1}{1 - e^{-\iota k_{i,j}(4-2\sqrt{2})\Delta x}} \tag{4.25}$$

And used for:

$$u_{1,J} = w_1 u_{II-2,J} + w_2 u_{II-1,J} \tag{4.26}$$

Now all representing ray components except for the required component are removed from the residual, as is shown in the lower right of figure 4.4. All horizontal and vertical Ray directions can be obtained in a similar way.

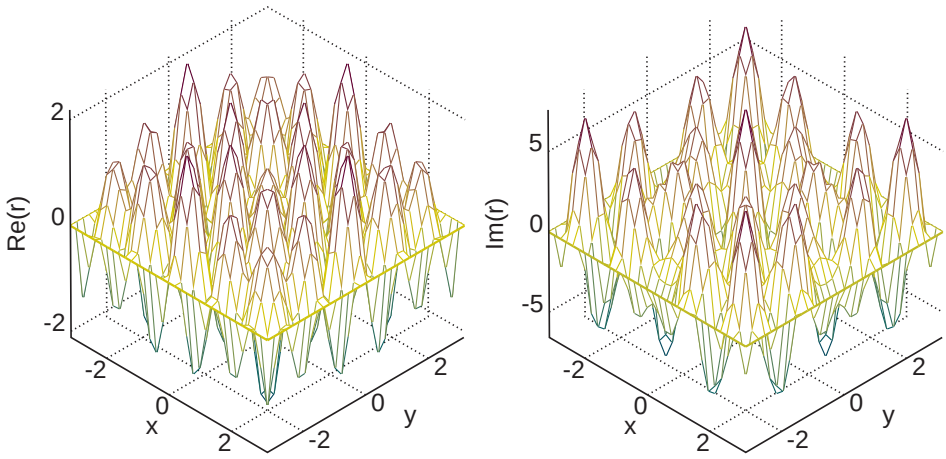

Figure 4.5: The test residual, as defined in equation 4.27, on the separation level

If separation is not performed parallel it is possible to remove obtained ray components from the residual before performing the separation process for a certain direction.

The diagonal ray-directions have a slightly different separation method. These directions will be separated using the horizontal grids, and in a last coarsening step rotated to a diagonal grid. To perform this last coarsening step, only one coarsening in each direction is allowed during the separation process. This requires one weighting in the x-direction with asymmetric boundary weighting, and one weighting in the y-direction with asymmetric boundary weighting. The principle however remains the same, and oscillatory components will systematically be removed with weighting.

4.2.2 Separation results

To show the performance of the 2D separation scheme, results will be shown for the horizontal ray direction 0 and the diagonal ray direction 1. A test residual is created on the level where separation is performed. In figure 4.5 the test residual is shown for a test residual that is written as:

$$r = \sum_{n=0}^{7} e^{\iota k \xi_n} \tag{4.27}$$

In figure 4.7 the resulting right hand sides for rays 0 and 1 are shown. As all primary directions have residual amplitude of 1, a same amplitude is to be expected in the resulting right hand side. Both rays in figure 4.7 show an amplitude of 1 in the domain of interest. Outside the domain of the wave

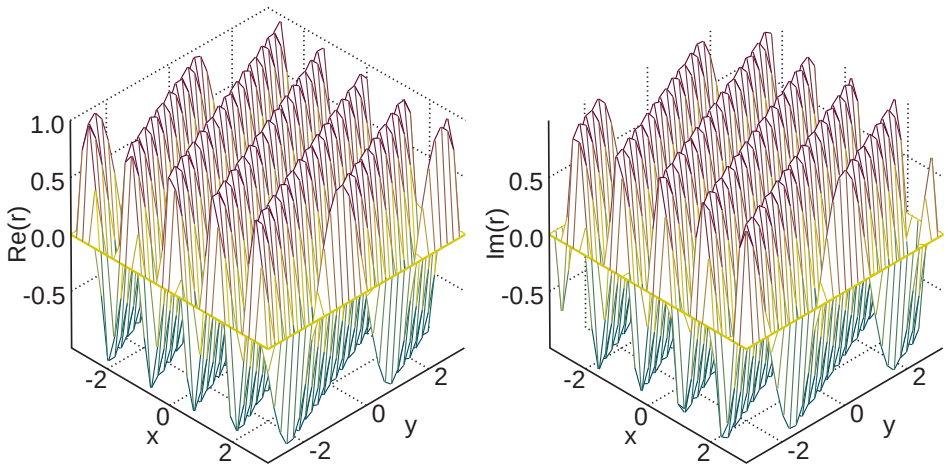

Figure 4.6: The test residual, as defined in equation 4.28, on the separation level

function the right hand side is expected to be zero in this case. It can be seen that for the main directions the residual can be separated exactly.

Not only the main directions have to be represented by the ray equations. The ray directions in between can influence the right hand side. The influence of a direction exactly between directions 0 and 1 is examined. Figure 4.6 shows a test residual that includes this direction and that can be written as:

$$r = e^{\imath k\left(x\cos\frac{\pi}{8}+y\sin\frac{\pi}{8}\right)} \tag{4.28}$$

The result of separation is shown in figure 4.8. The residual of a ray direction in between is now divided over several directions. The residual however not only influences the nearest rays, but also the other directions, with the used separation scheme. Further research is necessary to investigate the influence of these residuals on the overall convergence, and to investigate possibilities of other separation schemes. Such an alternative separation scheme could be to always use weighting with coarsening and to refine the result to the required ray level. Another alternative is to remove separated functions from the residual before performing separation for the next direction.

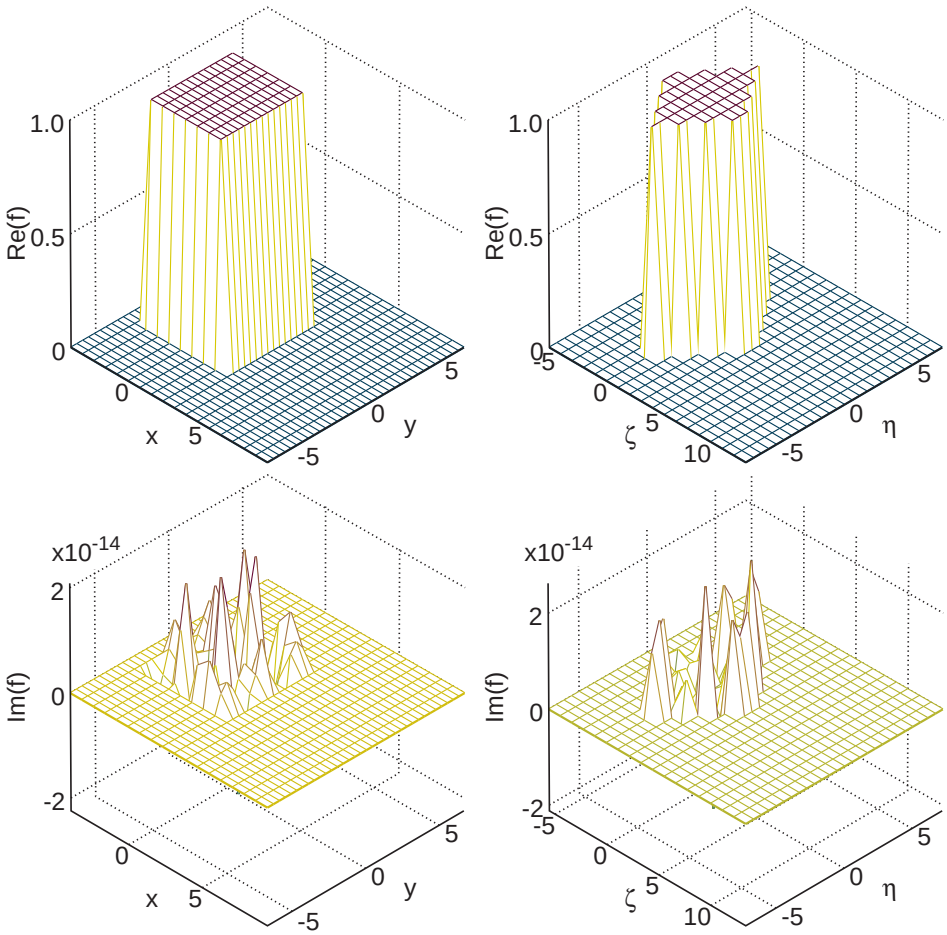

Figure 4.7: The right hand side with the amplitude of the 0(left) and 1(right) component determined with the separation scheme starting with a test residual as defined in equation 4.27

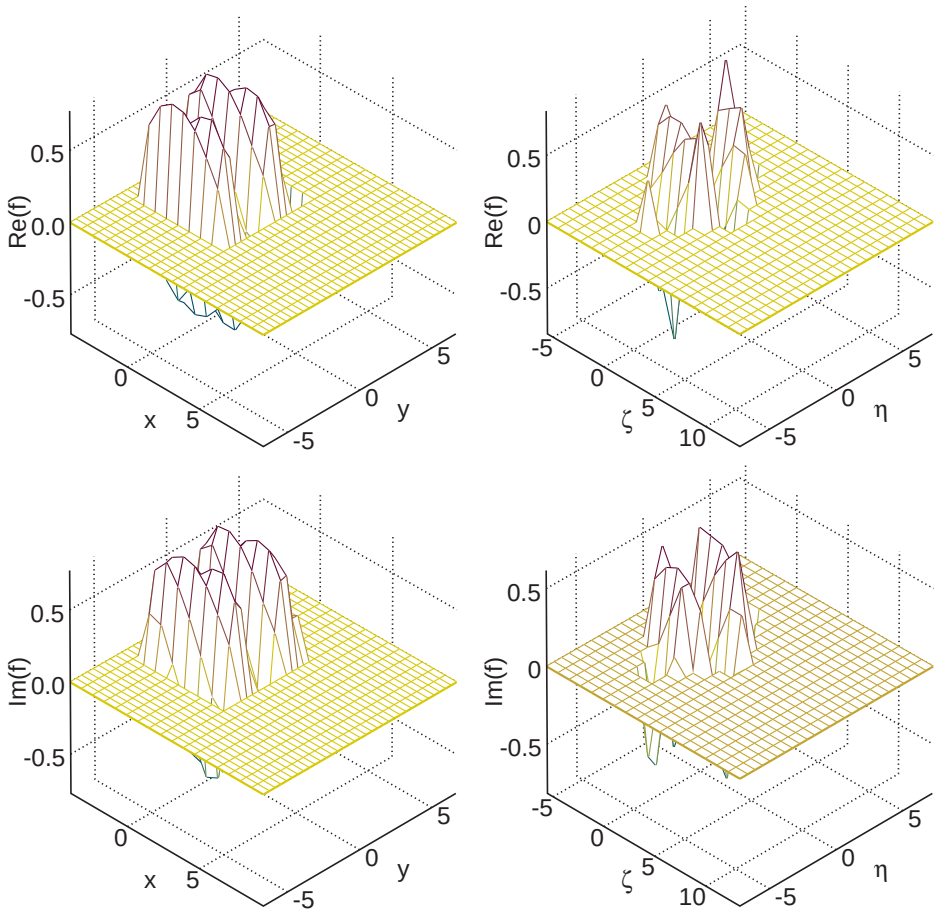

Figure 4.8: The right hand side with the amplitude of the 0(left) and 1(right) component determined with the separation scheme starting with a test residual as defined in equation 4.28

Chapter 5

Results for 1D-Helmholtz

In this chapter results will be presented for the Wave-Ray algorithm applied to the solution of 1D Helmholtz equation. First results for the homogeneous case with a constant wave-number will be shown. Next the the homogeneous case with a varying wave-number will be considered, followed by the non-homogeneous case with a constant wave-number. Finally, results will be presented for the non-homogeneous case with a varying wave-number.

5.1 Homogeneous case with constant wave-number

Analytic solutions of the 1D Helmholtz equation for homogeneous cases with constant wave-number are easy to obtain. Therefore performance can be evaluated using not only the reduction of the residual but also convergence to the analytic solution, i.e. by monitoring the error. The error is taken as the difference between the approximate numerical solution and the analytic solution represented on the grid. Residuals and errors will be measured using the L_2-norm, defined as:

$$L_2 = \sqrt{\frac{1}{N}\sum_{i=0}^{N} \Delta_i \bar{\Delta}_i} \tag{5.1}$$

with Δ_i the value of the variable, and $\bar{\Delta}_i$ its complex conjugate.

First single grid relaxation is used for the problem with Dirichlet boundary conditions in the case of $k = 5.3\left[\mathrm{m}^{-1}\right]$. Figure 5.1 shows the approximation of the solution after 10^5 and 10^7 relaxations. It can be observed that the information contained in the boundary conditions propagates very slowly into the domain. The boundary conditions determine the magnitude of the characteristic component, i.e. the solution to the homogeneous equation. Their dominance of the convergence behaviour can be seen more clearly when such components are taken as initial solution. This is illustrated in figure 5.2, where the residual norm is presented for both cases with zero as initial condition and the analytical solution as initial condition.

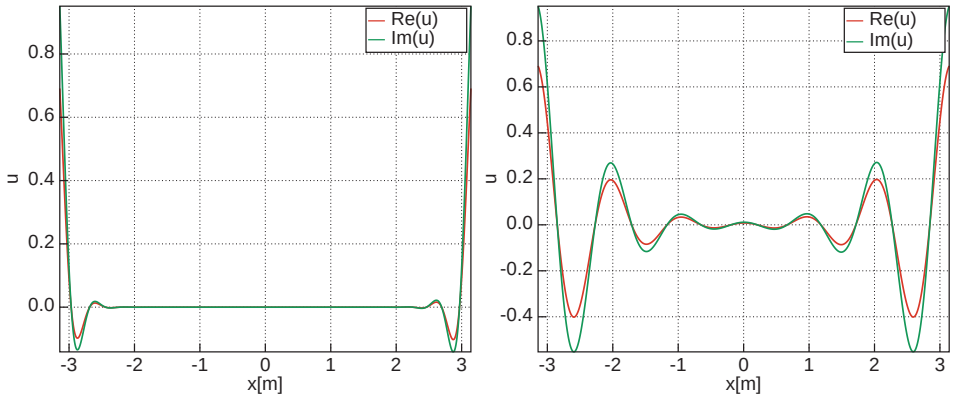

Figure 5.1: The real and imaginary part of the approximation to the solution $u(x)$ after 10^5(left) and 10^7(right) relaxation sweeps for $k = 5.3\left[\mathrm{m}^{-1}\right]$ for $L = 2\pi\,[\mathrm{m}]$ on a grid with 1025 points

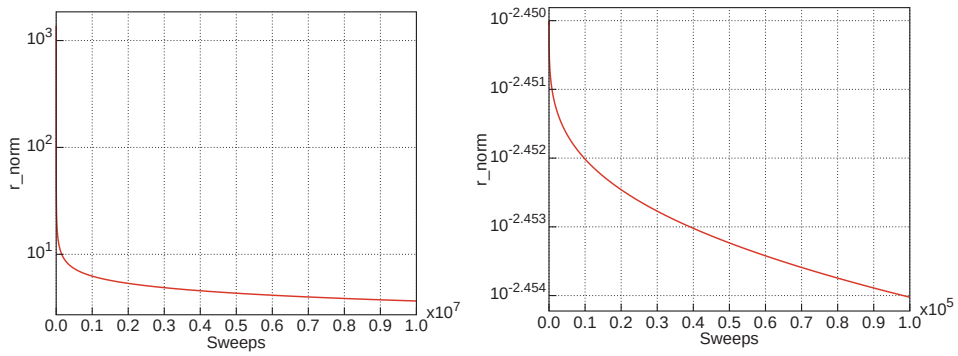

Figure 5.2: Single grid residual norm as a function of the number of sweeps for different initial approximations for $k = 5.3\left[\mathrm{m}^{-1}\right]$. Left the initial solution is zero and right the analytical solution is used as initial condition

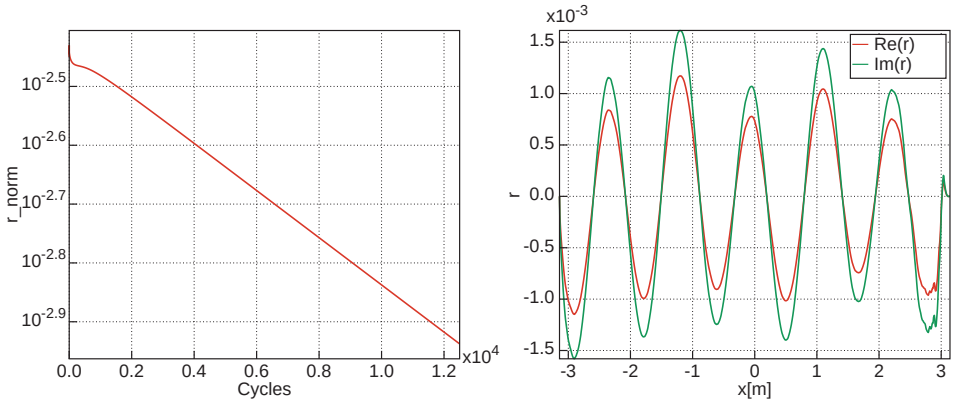

Figure 5.3: The residual norm depending on the number of cycles(left) and the residual $r(x)$ after 12500 cycles(right) using Wave Cycles for $k = 5.3\left[\mathrm{m}^{-1}\right]$

The convergence of the process can be accelerated by standard Multi-Level techniques, i.e. the Wave Cycle. In figure 5.3 the residual after 10^5 cycles as a function of x and the residual norm as a function of the number of sweeps are presented. The convergence rate is much higher than for single grid relaxation, but compared to what one obtains for elliptic problems very slow. The residual shows that the principal components indeed remain, which shows the need for separate treatment of these components as is done in the Wave-Ray scheme. The number of cycles used is lower than the number of relaxation sweeps used for the single grid scheme. Although a Multi-Level cycle is computationally more expensive then a relaxation, therefore, for a comparison with single grid relaxations, the number of cycles used is lower then the number of single grid relaxation sweeps. A crude estimate, including the work of restrictions and corrections, is that one cycle is about eight times as expensive as one sweep, see also Van Emden [3] for some crude workload estimates.

Next, the wave-ray scheme is applied to the solution of the same problem. The results are presented in figures 5.4, 5.5 and 5.6. Although the residual in figure 5.4 still shows the principal component, it is near zero. In figure 5.5 the residual norm is presented. The residual norm shows that after about sixty cycles the residual is reduced to machine accuracy. The amplification rate of the residual, also shown in figure 5.5, shows that the residual norm is amplified by about 0.6 per cycle for the major part of the process. This is a good performance but not as low as the LMA indicates as should be feasible. One possible reason is that the boundary conditions change a little each cycle. Another possible reason is that the number of relaxations on coarse grids is not high enough to justify the predicted asymptotic convergence rate.

Finally, the error norm and the ray amplitudes are presented in figure 5.6. The error norm reaches its final value in only a couple of cycles and is relatively

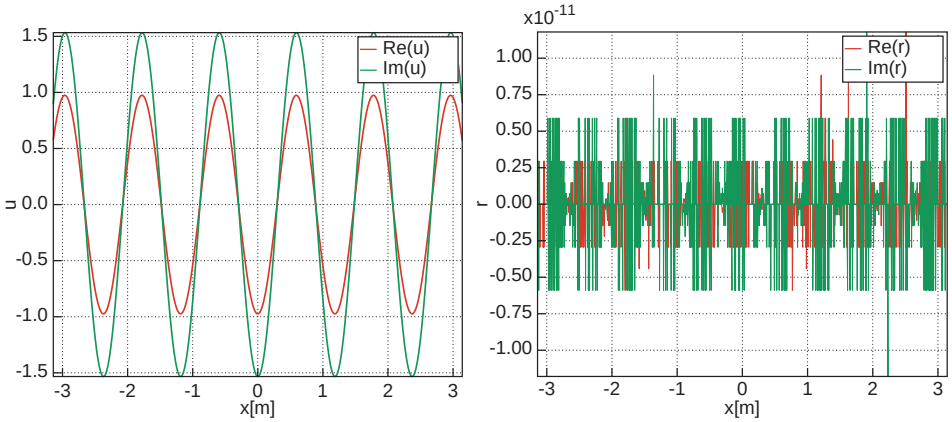

Figure 5.4: The approximation to the solution $u(x)$(left) and the residual $r(x)$(right) after 100 Wave-Ray cycles for $k = 5.3\left[\mathrm{m}^{-1}\right]$

high compared to the error in the standard scheme. This is, among others, caused by the correction of the boundary conditions due to the phase error, and can be reduced by using finer grids. The ray amplitudes show jumps at the boundaries of the domain, and constant values outside the domain. Inside the domain a slight slope can be observed. This slope is introduced into the ray solution by the phase error of the wave solution. Overall, the Wave-Ray algorithm provides an efficient numerical solution.

To investigate the influence of a large number of points, required when the wave-number is large, on the performance of the Wave-Ray scheme, the wave-number is increased to $k = 1000.16789\left[\mathrm{m}^{-1}\right]$ in the same domain of $L = 2\pi\,[\mathrm{m}]$. In figure 5.7 and 5.8 the results are presented. Although the amplification factor for the residual norm is a bit more variable than for the lower wave-number, it is still about 0.6 for most of the cycles. Machine accuracy is reached in about fifty cycles with a residual norm of $r_{\mathrm{norm}} = 9 \cdot 10^{-7}$. This result shows that the performance of the Wave-Ray algorithm is independent of the wave-number. Note that for these high wave-numbers a standard Multi-Level algorithm would fail to reach machine accuracy.

In figure 5.8 the error norm and the resulting ray amplitudes are shown. The error norm reaches its final value in just a few cycles. This value is twice as large as for the case of a low wave-number. Considering the greatly increased number of waves in the domain and its resulting phase error, this difference is not very high. The figure for the ray amplitudes again shows a slope due to a phase error correction, and this is better visible than with a low wave-number. It also shows that the left and right ray amplitude functions cross each other off-centre. This is, among others, caused by the chosen relaxation direction, which causes the amplitude of residuals to be x-dependant.

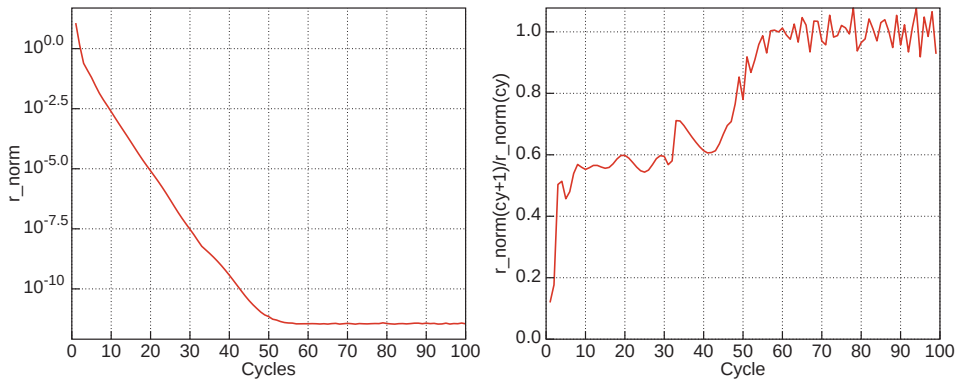

Figure 5.5: The residual norm depending on the number of cycles(left) and the amplification rate of the residual norm per cycle(right) using Wave-Ray cycles for $k = 5.3\left[\mathrm{m}^{-1}\right]$

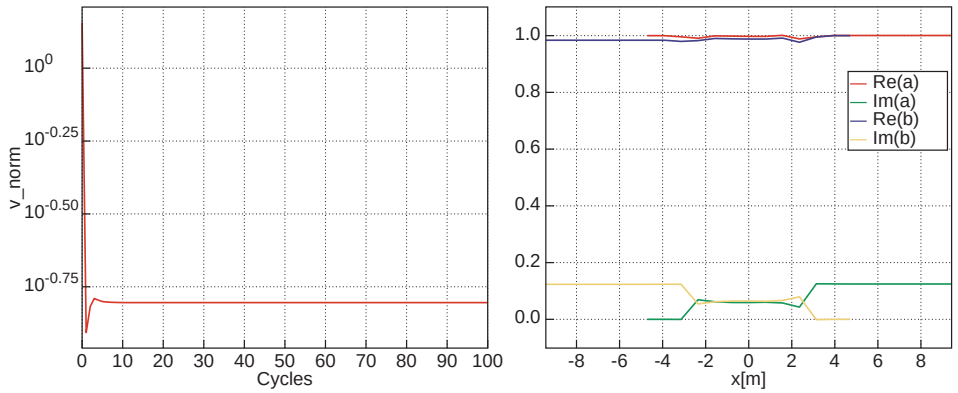

Figure 5.6: The error norm depending on the number of cycles(left) and the ray amplitudes $a(x)$ and $b(x)$ after 100 cycles(right) using Wave-Ray cycles for $k = 5.3\left[\mathrm{m}^{-1}\right]$

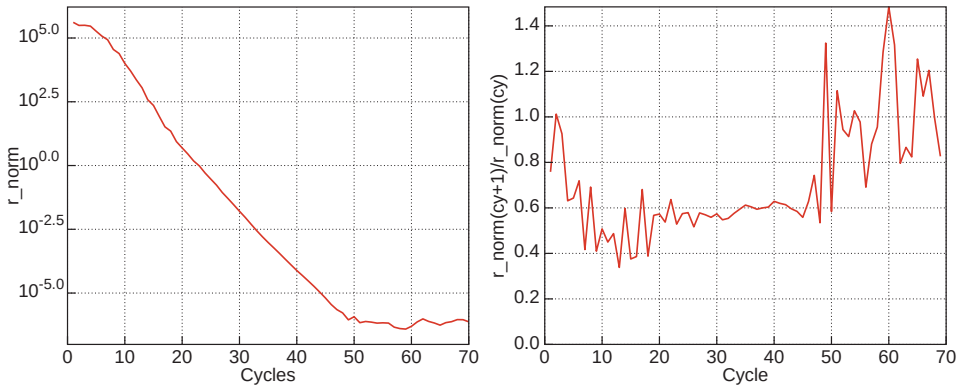

Figure 5.7: The residual norm depending on the number of cycles(left) and the residual norm amplification rate per cycle(right) for $k = 1000.16789 \left[\mathrm{m}^{-1}\right]$

Although the wave-ray scheme for such high wave-numbers works properly, the ray part becomes computationally expensive, as the ray-grid becomes rather large. With the current wave-number a coarse grid is required with 1571 points, and iterative methods on such large grids again show a stalling residual reduction rate. Therefore it is recommended for large wave-numbers to introduce a Multi-Level scheme for the solution of the ray equations. When using standard Gauß-Seidel relaxation to solve the equations iteratively, under-relaxation is required for high wave-numbers to obtain a stable process. In the current solution method an under-relaxation factor $\omega = 0.75$ is used. It is to be expected that a Multi-Level scheme for the solution of the ray-equations also improves the stability, as low frequency oscillating factors are reduced more efficiently.

5.2 Varying wave-number

Two cases of varying wave-number will be be considered. First, a discontinuous wave-number. An example of a discontinuous wave-number is when sound propagates through different media, e.g. a balloon with helium in a room filled with normal air. Note that the ray equations can be written in such a way that derivatives to the products of ka and kb are required instead of derivatives to k itself, which are very smooth or even continuous. Secondly, a smoothly varying wave-number. A practical example of such a case is when due to smooth temperature variations in the air.

An example of a 1D case in which a jump in the wave-number occurs is sound propagation in a pipe where, at a specific location, a freely vibrating membrane is positioned which separates air on one side from carbon dioxide on the other side. The speed of sound for these media differs by a factor 1.3.

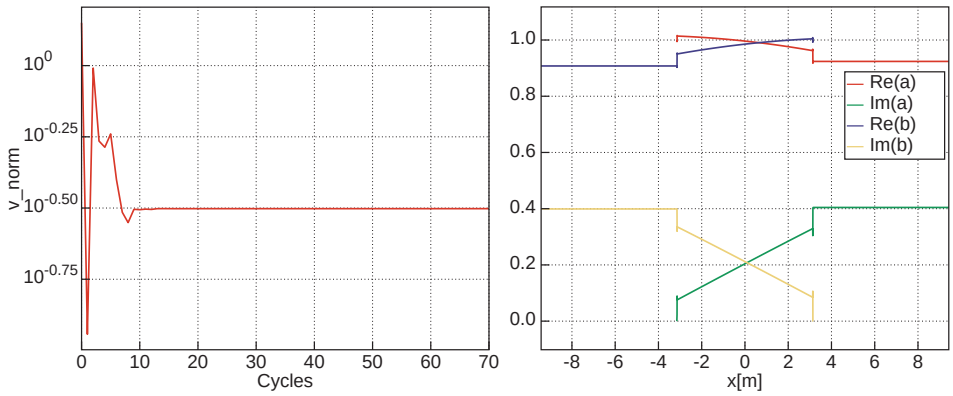

Figure 5.8: The error norm depending on the number of cycles(left) and the ray amplitudes $a(x)$ and $b(x)$(right) for $k = 1000.16789 \left[\mathrm{m}^{-1}\right]$

The discontinuity in wave-number results in two different standing waves in the two parts of the domain. This is realized by reflection and transmission at the interface.

Figure 5.9 shows results for the case, with $k = 8 \left[\mathrm{m}^{-1}\right]$ for $x < \frac{\pi}{16}$ and $k = 10.4 \left[\mathrm{m}^{-1}\right]$ otherwise. As can be seen the solution has a higher frequency in the right part of the domain. This is explained by the slower propagation of the sound in this part. Consequently the frequency in space is larger. The amplitude of the solution decreases significantly over the membrane. The interface causes the amplitude of the imaginary part of the solution to be reduced in the whole domain. The amplitudes for the ray functions clearly show the effect of a jump in the wave-number at $x = \frac{\pi}{16}$ [m], although the jumps in the amplitudes are slightly more difficult to observe due to phase error corrections.

The reduction rate of the residual norm shows a decreased performance compared to the case of a constant wave-number, i.e. an amplification factor of 0.8 instead of 0.6. This is caused by the choice of the magnitude of the jump in the wave-number. If the jump is chosen very large and Δx is kept constant, it is not possible to choose an optimal grid size based on $k\Delta x$. This can be solved by using a varying mesh size in the domain. However, this leads to more complicated restriction and correction schemes, or to the necessity to use algebraic multi-grid. Another possibility is to use the maximum value of the wave-number to determine the mesh size instead of using the average, as was done here. For the position of the jump, chosen here, the scheme remains stable up to a ratio $\frac{k_{\text{right}}}{k_{\text{left}}} \approx 1.5$, when using the average wave-number to determine the grid size such that $\bar{k}\Delta x = 1$ on the separation level.

As an example of a smoothly varying wave-number a case is considered where a heat source in the centre causes a varying temperature in the medium.

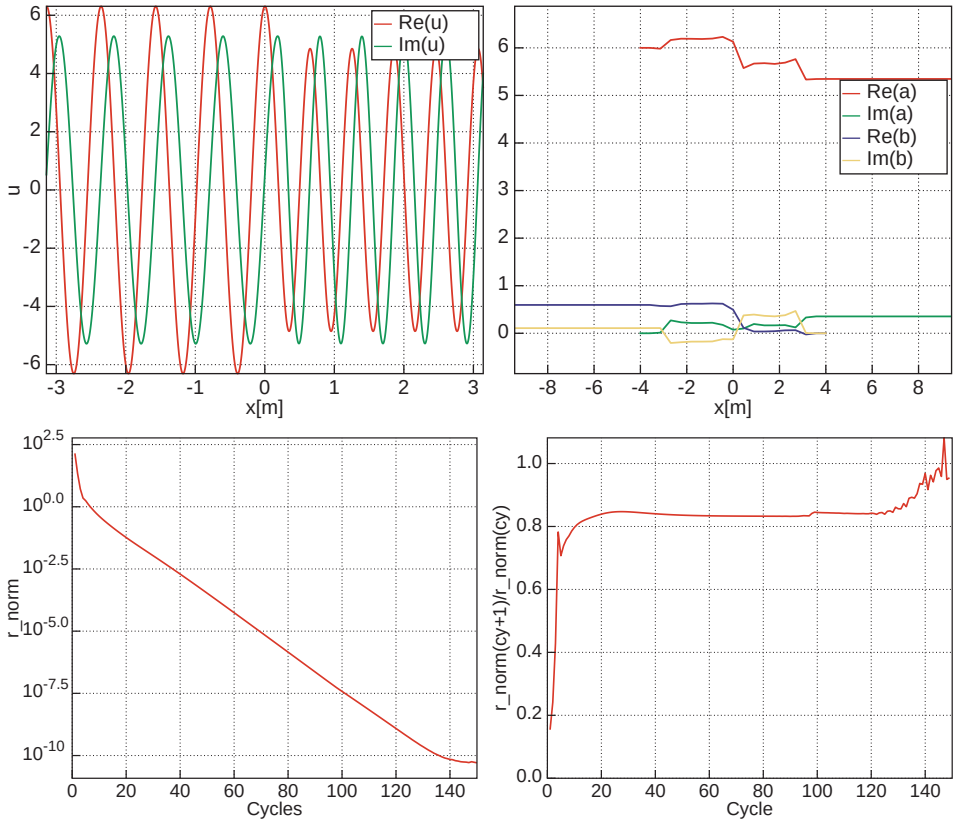

Figure 5.9: Results for a jump in the wave-number, with $k = 8\left[\mathrm{m}^{-1}\right]$ for $x < \frac{\pi}{16}\,[\mathrm{m}]$ and $k = 10.4\left[\mathrm{m}^{-1}\right]$ otherwise; First $u(x)$ in the left upper corner, then the ray amplitude functions $a(x)$ and $b(x)$ in the right upper corner, next the residual norm depending on the number of cycles in the lower left and the amplification of the residual norm per cycle in the lower right

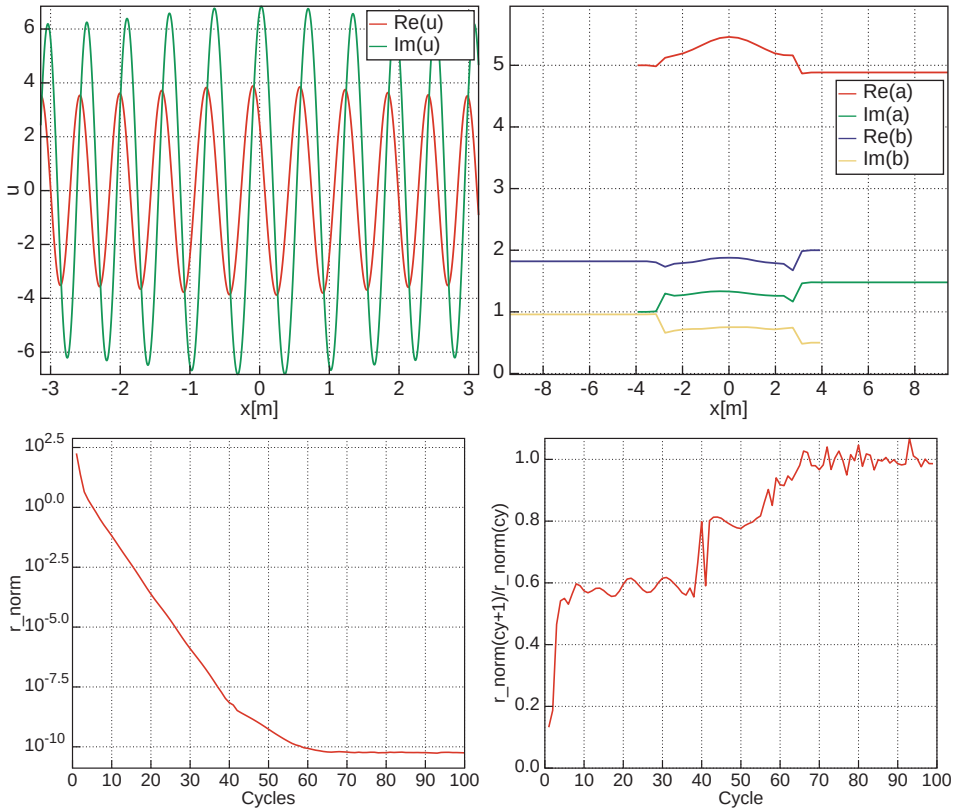

Figure 5.10: Results for $k = 10.3\,(1 - 0.1\cos(x))\left[\mathrm{m}^{-1}\right]$. First the approximation to $u(x)$ in the upper left, next the ray amplitude functions $a(x)$ and $b(x)$ on the right. Subsequently, the residual norm depending on the number of cycles in the lower left, and finally, the amplification of the residual norm per cycle in the lower right

A higher temperature in the centre of the domain causes the speed of sound to increase and therefore the wavelength in space of the travelling wave for a specific frequency increases too. This causes the wave-number to decrease in that part of the domain.

Results for such a case are presented in figure 5.10. The wave-number is chosen to vary with x as $k(x) = 10.3\,(1 - 0.1\cos(x))\left[\mathrm{m}^{-1}\right]$. The approximation to the solution has an increased wavelength in the centre of the domain and a decreased wavelength in the other parts compared to the case of a constant wave-number. It can also be observed that the amplitude increases with increasing wavelength. The performance of the Wave-Ray scheme in terms of the residual amplification factor is similar to the case of a constant wave-number. However, when the differences in the wave-number over the domain increase, the residual amplification factor increases. This is the same effect as observed for the discontinuous wave-number. Again the solution is to either tune the mesh size for optimal performance or to use a variable mesh sizes to keep $k\Delta x$ constant.

5.3 The non-homogeneous case

As an example of a non-homogeneous case the situation of a non-zero forcing at $x = 0$ is considered. Figure 5.11 shows the results obtained for this case. The forcing term, representing a source of vibration, induces a wave to the left and one to the right initiating at $x = 0\,[\mathrm{m}]$. This can be observed in both the approximation to the solution and in the approximation to the ray-amplitudes. Due to the wave-number of $k = 10\left[\mathrm{m}^{-1}\right]$, five wave-periods can be seen on both sides of the source. The residual amplification per cycle shows a similar performance as for the homogeneous case, as could be expected.

As a second example, the case of a smoothly varying forcing term is considered. The forcing is chosen as $f(x) = 40\cos 2x + 80\imath\sin x$. The unit of the forcing is the unit of the variable to be solved divided by square meter, and it will therefore be omitted. The results for this case are presented in figure 5.12. It can be observed that the real and imaginary part of the solution follow the respective parts of the forcing. It can also be observed that the amplitudes of the rays remain almost constant in the domain of interest, due to the phase error correction. The performance of the Wave-Ray algorithm is not effected by the smoothly varying source terms.

5.4 General case

Both a forcing and a non-constant wave-number have been tested separately. As a final example a case will be presented with a discontinue but otherwise smoothly varying wave-number and forcing terms. In the example forcing

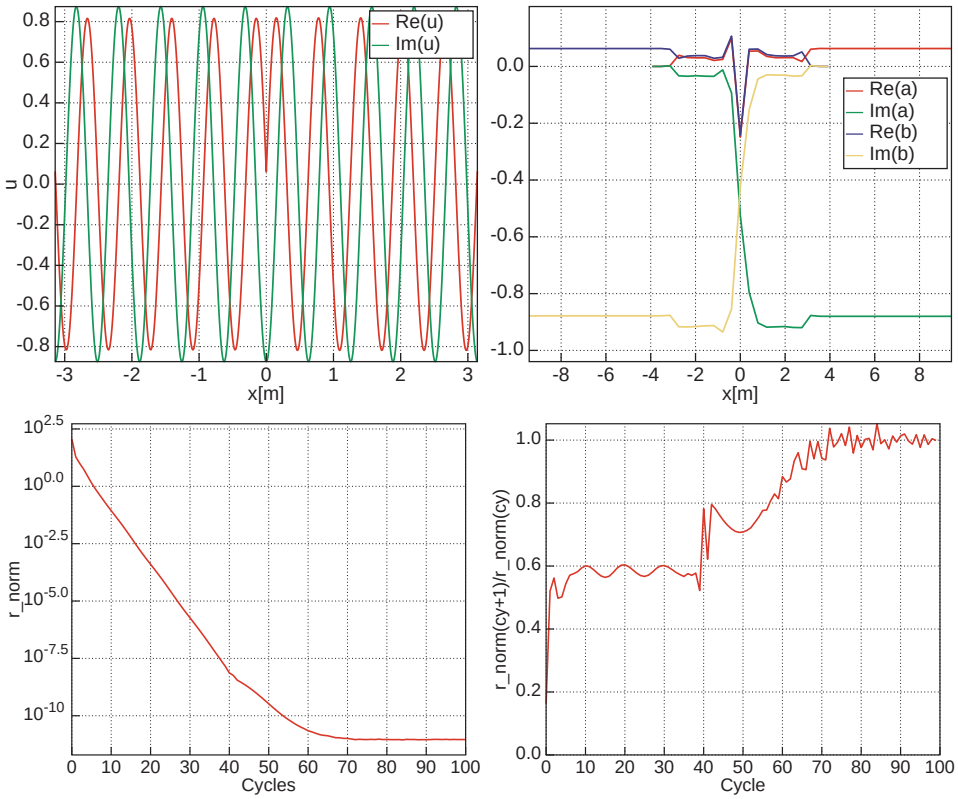

Figure 5.11: Results for a source at $x = 0\,[\mathrm{m}]$, $k = 10\left[\mathrm{m}^{-1}\right]$. First the approximation to $u(x)$ in the upper left, next the ray amplitude functions $a(x)$ and $b(x)$ on the right. Subsequently, the residual norm depending on the number of cycles in the lower left, and finally, the amplification of the residual norm per cycle in the lower right

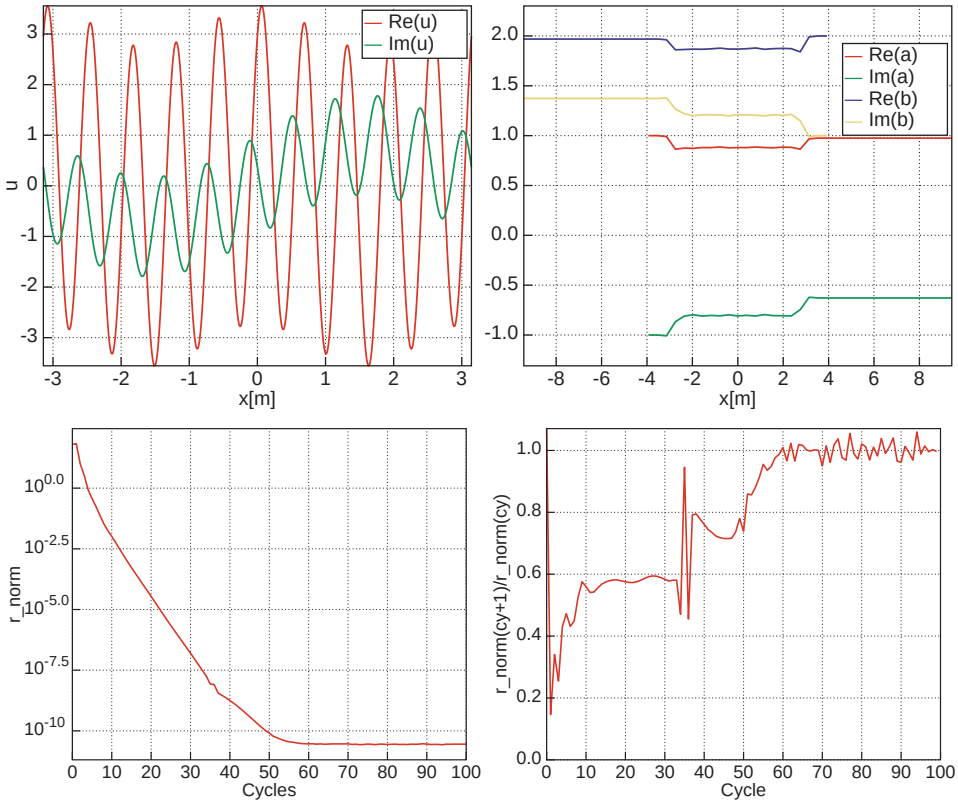

Figure 5.12: Results for $f(x) = 40\cos 2x + 80\imath \sin x$. First the approximation to $u(x)$ in the upper left, next the ray amplitude functions $a(x)$ and $b(x)$ on the right. Subsequently, the residual norm depending on the number of cycles in the lower left, and finally, the amplification of the residual norm per cycle in the lower right

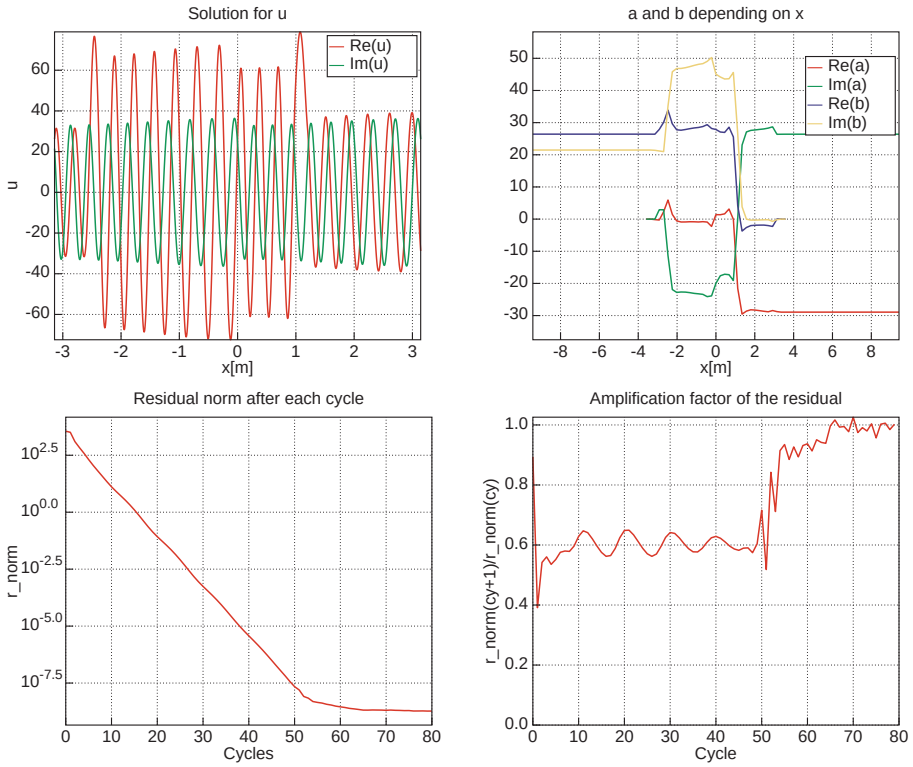

Figure 5.13: Results for a case with sources and non-constant wave-number. First the approximation to $u(x)$ in the upper left, next the ray amplitude functions $a(x)$ and $b(x)$ on the right. Subsequently, the residual norm depending on the number of cycles in the lower left, and finally, the amplification of the residual norm per cycle in the lower right

terms are located at $-2.6 < x < -2.4\,[\mathrm{m}]$ and $1 < x < 1.2\,[\mathrm{m}]$. The wave-number is chosen to be $k = 10.3\,(1 - 0.1\cos(x))\left[\mathrm{m}^{-1}\right]$ for $x < 0\,[\mathrm{m}]$ and $k = 10.3\,(1 + 0.1\cos(x))\left[\mathrm{m}^{-1}\right]$ for $x > 0\,[\mathrm{m}]$. Both ray amplitudes are chosen to be zero at their respective boundaries, i.e. no other sources of sound are outside the domain of interest.

In both the solution and the ray amplitudes different aspects can be observed. Jumps in amplitude occur at the locations of the sources and at the location of the discontinuity in wave-number. The solution also shows the influence of the smooth variations of the wave-number. Just as for the cases of a varying wave-number, considered earlier, the residual amplification factor increases when the variation in wave-number is too large. This effect can, again, be overcome by better tuning of the mesh size, or by using a variable mesh size.

The performance of the Wave-Ray Multi-Level scheme has been illustrated for different characteristic problems in 1D. It was shown that, as long as a

proper mesh size is chosen and the variations in the wave-number do not become too large, a residual reduction of almost a factor two per cycle can be obtained. Moreover, within a few cycles an approximation can be obtained with an error within discretization error. The scheme is a major improvement over standard iterative and Multi-Level schemes. Furthermore it provides for adapting boundary conditions to include sources within and outside the domain of interest.

Chapter 6

Results for 2D-Helmholtz

With a working 1D wave-ray scheme and a working separation scheme, the 2D wave-ray scheme can now be considered. However, compared to the 1D case, the implementation of the Wave-Ray scheme for 2D is much more involved.

For example, the boundary now consists of multiple neighbouring points. This implies that boundary points also need to be restricted to coarser grids and vice versa need to be corrected with an interpolation scheme. As in the standard scheme no relaxation takes place on these points, the resulting boundary is not smooth when introducing the boundary conditions on the coarse grid.

Preliminary results, having tackled several problems, show a Wave-Ray scheme working for four directions for the relatively low $k = 2.6 \left[\mathrm{m}^{-1}\right]$ on a domain of $2\pi \times 2\pi \left[\mathrm{m}^2\right]$. A wave-number $k = 2.6 \left[\mathrm{m}^{-1}\right]$ on a domain of $2\pi \times 2\pi \left[\mathrm{m}^2\right]$ still requires a grid of 512×512 points and is therefore already demanding for the computer. As a test case the rays, in these four directions, all have an amplitude of 1 as boundary condition, with the wave-number $k = 2.6 \left[\mathrm{m}^{-1}\right]$ in a domain of $2\pi \times 2\pi \left[\mathrm{m}^2\right]$. The solution obtained with this scheme is presented in figure 6.1, accompanied by the residual at the separation level. The solution is indeed a combination of four rays. The residual on the separation level is smooth and is a combination of four rays in the diagonal directions. This is to be expected as the diagonal waves are not reduced efficiently by the currently used wave-ray scheme for four directions.

Figure 6.2 shows the residual norm and its amplification factor. The four principal directions currently treated in the Wave-Ray scheme, are removed from the residual in only a few cycles. The amplification factor is still high in most part of the solution process, however, up to 20 cycles a reduction rate of 0.7 is reached. The four other principal directions not yet treated with the currently used scheme cause the residual reduction to stall. However, it still reaches machine accuracy after enough cycles. As only four directions are reduced efficiently, addition of the diagonal rays should increase the performance significantly. At the moment however the addition of these rays is not yet implemented.

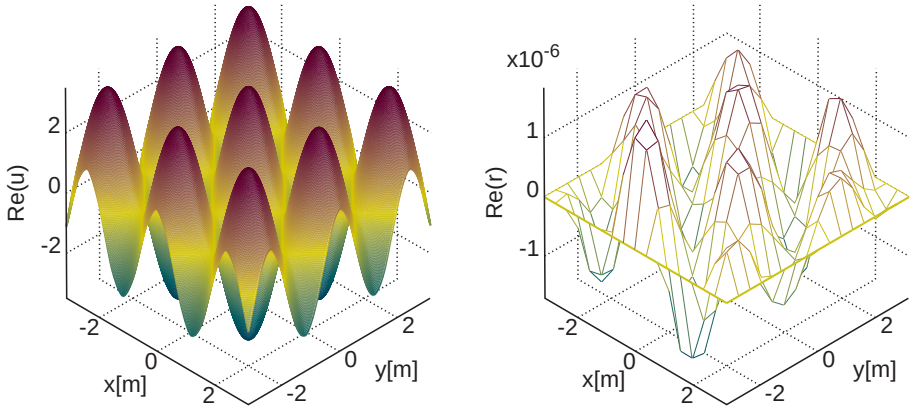

Figure 6.1: Approximation to $u\left(x,y\right)$ (left) and residual on the separation level $r\left(x,y\right)$ (right) for four rays in 2D with $k=2.6\left[\mathrm{m}^{-}1\right]$

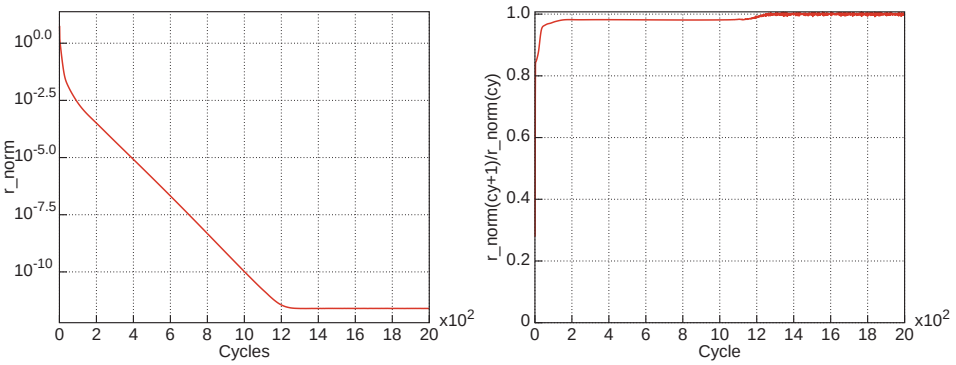

Figure 6.2: Residual norm depending on the number of cycles(left) and the residual amplification per cycle(right) for four rays in 2D with $k=2.6\left[\mathrm{m}^{-1}\right]$

As mentioned, the boundary points need special attention. There are multiple options to tackle this problem. One option is to use an extended domain in the Ray cycle, with one extra mesh size in all directions. This will lead to a scheme including the original boundary points in the relaxation process. Such a scheme is troublesome to implement due to negative indexes. Another option is to introduce the boundary points on each grid by interpolated ray amplitudes multiplied with its exponential function. Although this scheme should give a smooth boundary, the interpolation of ray amplitudes and multiplication with their principal component require a lot of work and extra data to be stored. Yet another option is to use higher order interpolation schemes. This can result in a smooth boundary, however, in the corners a choice has to be made to use decentralized interpolation, or to use lower order interpolation. Furthermore, higher order interpolation can introduce highly oscillatory error components into the scheme.

The option with an extended boundary is chosen to be used in the Wave-Ray scheme. Implementation of these boundaries in the Wave-Ray scheme leads to altered restriction and correction schemes to include the extension of the domain. Although the domain is extended on each level with one point in all directions, the dimensions of the domain become larger each coarser grid due to increasing mesh size. The domains of the Ray-equations also have been extended to be able to correct the new boundary.

Another problem that arises is that the separation does not work as efficiently as desired for errors not in one of the chosen ray-directions. These ray directions introduce oscillations in the residual finally causing the ray solutions to become oscillating and causing the total scheme to become unstable. To solve this problem for the horizontal and vertical directions, an extra weighting step is performed on the separated residual in the perpendicular direction. A simple $\begin{bmatrix} 1 & 2 & 1 \end{bmatrix}$ weighting scheme produces a ray right hand side without the undesired oscillations.

A third problem that arises when introducing the wave-ray scheme in 2D is that, using the same number of relaxations per level as for 1D, the residual is not yet ready for separation. Either more wave-cycles need to be performed to obtain usable residuals, or more relaxations per level in the wave-cycle need to be performed. It has been chosen to increase the number of relaxations per level with a factor two, leading to residuals that can be separated.

Chapter 7

Conclusions and recommendations

Standard iterative solution methods for the discretized Helmholtz equation in (semi-)infinite domains, discretized using a Finite Difference Method, are inefficient. A Multi-Level solution increases the performance of standard iterative methods. As is shown, for the Helmholtz equation, a standard Multi-Level scheme is not capable of reducing the principal error components efficiently. Therefore a wave-ray scheme has been introduced, not only to restore the performance of the Multi-Level scheme, but also to implement radiation boundary conditions representing incoming rays from the far field.

For 1D a working wave-ray scheme has been developed and its performance has been demonstrated. For most part of the solution process a wave-ray cycle reduces the residual by a factor two. Moreover, after only a few cycles the approximation of the solution is within the level of the discretization error. The residual reduction rate is independent of the wave-number, but large variations in the wave-number can reduce the efficiency of the wave-ray scheme significantly. For large variations of the wave-number, the mesh size can be tuned to restore its performance when the variations are not too large. If the variations are too large, alternative schemes will have to be used, e.g. variable mesh size per grid to obtain a constant kh.

The 1D scheme has been shown to be stable and very efficient, for wave-numbers up to $k = 1000 \left[\mathrm{m}^{-1}\right]$ in a domain of $L = 2\pi\,[\mathrm{m}]$. Results have been obtained for both smooth and discontinuous wave-number and also for the non-homogeneous case.

For the 1D Helmholtz equation two different separation schemes have been tested. Separation using standard full weighting is shown to be inefficient for large wave-numbers. Separation with calculated weighting factors can separate principal components more efficiently and is recommended.

A separation scheme has been developed for the 2D case. Separation of the eight ray-directions can be performed very efficiently. Separation of principal

components in other directions introduce oscillations in the resulting separated residual and therefore needs more attention.

Using the separations scheme, a wave-ray scheme has been developed that uses four of the ray-directions. To obtain a smooth solution, including a smooth boundary, the border of the domain of interest is extended with one point. The number of relaxations in the wave-cycle need to be reduced to obtain a residual that can be separated. As only four directions have been used, principal components in the diagonal directions are not reduced efficiently. This reduced the efficiency of the current wave-ray scheme.

Although the principle of the wave-ray scheme has been shown, further research into separation in 2D is required to be able to improve stability of the scheme. It is also recommended to test higher order interpolation for the boundaries instead of extending the computational domain of the equation, to be able to compare both methods. When a stable wave-ray scheme is obtained using all eight ray-directions, sources can be introduced. Further research also needs to be done into the function for the phase of the solution $s_\theta\left(\xi,\eta\right)$. This can be used to test the wave-scheme for a varying wave-number.

Following the development of a working 2D wave-ray scheme has been developed for arbitrary forcing and varying wave-number, the scheme can be extended to the 3D case. For the extension of separation routines and calculation of the phase functions from 2D to 3D, many routines retain the basic principle. The extra dimension introduces its own unique problems, for instance, the number of rays enabling the representation of the solution needs to be determined.

For experimental purposes it is recommended to experiment using for instance air and carbon dioxide, and not air and helium as the difference in speed of sound is preferred to be not too high. When experiments validate the scheme, the scheme can be adapted for larger variations in wave-number and arbitrary domains including domains with objects inside the domain of interest.

Bibliography

[1] Irene Livshits and Achi Brandt. Accuracy properties of the wave-ray multigrid algorithm for helmholtz equations. *Siam Journal on Scientific Computing*, 28(4):1228–1251, 2007.

[2] Isaías Hernández Ramírez. *Multilevel Multi-Integration Algorithm for Acoustics*. PhD thesis, University of Twente, Enschede, The Netherlands, 2005.

[3] Ellen van Emden. A multilevel solver for acoustical problems, wave-ray algorithm of the 1d helmholtz equation. Master's thesis, University of Twente, Enschede, The Netherlands, January 2008.

Nomenclature

Roman

Symbol	Units	Description
a	$[-]$	Amplitude of right travelling ray in 1D
a^h	$[-]$	Discrete solution of a
$\tilde{a}^h$	$[-]$	Approximation of a^h from previous Ray Cycle
$\hat{a}^h$	$[-]$	Corrected approximation of a^h
a_θ	$[-]$	Amplitude of ray travelling in θ-direction
a_θ^h	$[-]$	Discrete solution of a_θ
$\tilde{a}_\theta^h$	$[-]$	a_θ^h obtained in last Ray Cycle
$\hat{a}_\theta^h$	$[-]$	Corrected a_θ^h obtained in current Ray Cycle
A	$[-]$	Boundary value right travelling ray
A_θ	$[-]$	Boundary function ray in θ-direction
$\tilde{A}$	$[-]$	Amplitude of Fourier component of $\tilde{v}^h$
$\hat{A}$	$[-]$	Amplitude of Fourier component of $\hat{v}^h$
$\mathbf{A}$	$[-]$	Matrix constructed from the operators on u^h
b	$[-]$	Amplitude of left travelling ray in 1D
b^h	$[-]$	Discrete solution of b
$\tilde{b}^h$	$[-]$	Approximation of b^h from previous Ray Cycle
$\hat{b}^h$	$[-]$	Corrected approximation of b^h
B	$[-]$	Boundary value left travelling ray
c_0	$\left[\mathrm{m\,s^{-1}}\right]$	Speed of sound reference state
D	$[-]$	The number of dimensions
E	$\left[\mathrm{m^2\,s^{-2}}\right]$	Total energy per unit mass
f	$[-]$	Amplitude of time dependent forcing, the unit depends on the required variable
f^h	$[-]$	Discrete representation of f
f^H	$[-]$	Coarse grid right hand side
f_a	$[-]$	Forcing of right travelling ray
f_b	$[-]$	Forcing of left travelling ray
f_θ	$[-]$	Forcing on ray in θ-direction
f_a^h	$[-]$	Discrete right hand side right travelling ray
f_b^h	$[-]$	Discrete right hand side left travelling ray

f_a^H	$[-]$	Discrete right hand side right travelling ray on the coarse grid
f_b^H	$[-]$	Discrete right hand side left travelling ray on the coarse grid
f_θ^h	$[-]$	Discrete right hand side ray in θ-direction
f_θ^H	$[-]$	Discrete right hand side ray in θ-direction on the coarse grid
$\mathbf{F}$	$\left[\mathrm{kg\,m^{-2}s^{-2}}\right]$	Density of the forcefield vector
$\mathbf{F}'$	$\left[\mathrm{kg\,m^{-2}s^{-2}}\right]$	Density of the forcefield perturbation vector
$\mathbf{F}_0$	$\left[\mathrm{kg\,m^{-2}s^{-2}}\right]$	Density of the forcefield reference state vector
g	$[-]$	Time dependency of the forcing
G	$[-]$	Time dependency of the pressure perturbation
h	$[\mathrm{m}]$	Mesh size for meshes with constant spacing
H	$[-]$	Coarse grid mesh size
$I_h^H\langle\rangle$	$[]$	Restriction operator
$I_H^h\langle\rangle$	$[]$	Interpolation operator
i	$[-]$	Index of discrete point in x-direction
I	$[-]$	Coarse grid index in x-direction
j	$[-]$	Index of discrete point in y-direction
J	$[-]$	Coarse grid index in y-direction
k	$[-]$	Index of discrete point in z-direction
K	$[-]$	Coarse grid index in z-direction
k	$\left[\mathrm{m}^{-1}\right]$	Wave-number related to the Fourier component
k^h	$\left[\mathrm{m}^{-1}\right]$	Discrete representation of the wave-number
$k_{1,\theta}$	$\left[\mathrm{m}^{-1}\right]$	Wave-number for θ-ray, experienced in x-direction
$k_{2,\theta}$	$\left[\mathrm{m}^{-1}\right]$	Wave-number for θ-ray, experienced in y-direction
L	$[\mathrm{m}]$	Length of the domain
L_2	$[]$	The so called L_2 norm
$L^h\langle\rangle$	$[-]$	Discretized PDE operator
$L^H\langle\rangle$	$[-]$	Coarse grid operator
n	$[-]$	Number of points in one direction
N	$[-]$	The total number of points
$\mathcal{O}$	$[-]$	Of the order of
p	$\left[\mathrm{kg\,m^{-1}s^{-2}}\right]$	Pressure
p'	$\left[\mathrm{kg\,m^{-1}s^{-2}}\right]$	Pressure perturbation
p_0	$\left[\mathrm{kg\,m^{-1}s^{-2}}\right]$	Pressure reference state
P	$\left[\mathrm{kg\,m^{-1}s^{-2}}\right]$	Amplitude of the time dependent pressure perturbation
p^h	$[-]$	Element on the diagonal of $\mathbf{A}$
$\mathbf{q}$	$\left[\mathrm{kg\,s^{-3}}\right]$	Heat flux vector
$\dot{Q}$	$\left[\mathrm{kg\,m^{-1}s^{-3}}\right]$	Time rate of volumetric heat addition
s	$[-]$	Phase of the rays in 1D

s_θ	$[-]$	Phase of ray travelling in θ-direction
$S_a\langle\rangle$	$[-]$	Separation operator for right travelling ray
$S_b\langle\rangle$	$[-]$	Separation operator for left travelling ray
t	$[\mathrm{s}]$	Time
$\mathbf{u}$	$\left[\mathrm{m\,s^{-1}}\right]$	Velocity vector
$\mathbf{u}'$	$\left[\mathrm{m\,s^{-1}}\right]$	Velocity perturbation vector
$\mathbf{u}_0$	$\left[\mathrm{m\,s^{-1}}\right]$	Velocity reference state vector
u	$[-]$	General unknown for the Helmholtz equation
u^h	$[-]$	Discrete solution
$\tilde{u}^h$	$[-]$	Given approximation to u^h
$\hat{u}^h$	$[-]$	Corrected approximation to u^h
$\bar{u}^h$	$[-]$	$\tilde{u}^h$, or $\hat{u}^h$ depending on used relaxation method and index
$\tilde{\tilde{u}}^h$	$[-]$	Given approximation to u^h using Kaczmarz
$\tilde{\tilde{u}}^h$	$[-]$	Once corrected approximation during a sweep
$\hat{\tilde{u}}^h$	$[-]$	Twice corrected approximation during a sweep
$\hat{\hat{u}}^h$	$[-]$	Fully corrected approximation during a sweep
u^H	$[-]$	Coarse grid solution
$\tilde{v}^h$	$[-]$	Error of given approximation
$\hat{v}^h$	$[-]$	Error of corrected approximation
w	$[-]$	Weighting factor for restriction
$\mathbf{x}$	$[\mathrm{m}]$	Position vector in space relative to a chosen origin
x	$[\mathrm{m}]$	First entity of $\mathbf{x}$
x_a	$[\mathrm{m}]$	Location of lower, left, boundary in x-direction
x_b	$[\mathrm{m}]$	Location of upper, right, boundary in x-direction
X	$[\mathrm{m}]$	Specific location in the x-direction
Δx	$[\mathrm{m}]$	Discrete step size in x-direction
$\tilde{x}^h$	$[-]$	The error of $\tilde{y}^h$
$\hat{x}^h$	$[-]$	The error of $\hat{y}^h$
y	$[\mathrm{m}]$	Second entity of $\mathbf{x}$
Δy	$[\mathrm{m}]$	Discrete step size in y-direction
$\mathbf{y}^h$	$[-]$	Dummy vector used for Kaczmarz relaxation
Δz	$[\mathrm{m}]$	Discrete step size in z-direction

Greek

Symbol	**Units**	**Description**
γ	$[-]$	Ratio of specific heats
δ_{ij}	$\left[\mathrm{kg\,m^{-1}s^{-1}}\right]$	Kronecker delta
δ^h	$[-]$	Correction value to correct given approximation to u^h

η	[m]	Axis perpendicular to θ-direction ray
H	[m]	Specific location in η-direction
θ	[rad]	Direction of ray relative to the x-axis
θ	[rad]	Fourier component frequency of the error in 1D
θ_1	[rad]	Fourier component frequency of the error in x-direction
θ_2	[rad]	Fourier component frequency of the error in y-direction
θ_3	[rad]	Fourier component frequency of the error in z-direction
ι	$[-]$	Imaginary part; $\iota^2 = -1$
λ	$\left[\mathrm{kg\,m^{-1}s^{-1}}\right]$	Bulk or volumetric viscosity coefficient
μ	$\left[\mathrm{kg\,m^{-1}s^{-1}}\right]$	Dynamic viscosity coefficient
μ	$[-]$	Error amplification factor
$\bar{\mu}$	$[-]$	Asymptotic convergence rate; $\max \mu$
ν	$[-]$	Number of relaxations to be performed
ξ	[m]	Axis in θ-direction ray
Ξ	[m]	Specific location in ξ-direction
ρ	$\left[\mathrm{kg\,m^{-3}}\right]$	Density
ρ'	$\left[\mathrm{kg\,m^{-3}}\right]$	Density perturbation
ρ_0	$\left[\mathrm{kg\,m^{-3}}\right]$	Density reference state
$\tau_{i,j}$	$\left[\mathrm{kg\,m^{-1}s^{-2}}\right]$	Viscous stress tensor
φ_a	$[-]$	Offset of the phase of right travelling ray in 1D
φ_b	$[-]$	Offset of the phase of left travelling ray in 1D
φ_θ	$[-]$	Offset of the phase of ray in θ-direction
ω	$\left[\mathrm{rad\,s^{-1}}\right]$	Frequency of the Fourier component of the harmonic forcing
ω	$[-]$	Relaxation factor

List of Figures

Appendix A

Gauß-Seidel for 1D-Helmholz

A.1 Derivation of the relaxation process

To derive the Gauß-Seidel relaxation for the Helmholtz equation, it is necessary to first start with the discrete Helmholtz equation. A second order accurate central difference scheme is used to numerically calculate the differential equation. For the Helmholtz equation this leads to:

$$\frac{u_{i-1}^h - 2u_i^h + u_{i+1}^h}{\Delta x^2} + {k_i^h}^2 u_i^h = f_i^h \tag{A.1}$$

Or with $p_i = \Delta x^2 {k_i^h}^2 - 2$:

$$\frac{u_{i-1}^h + p_i^h u_i^h + u_{i+1}^h}{\Delta x^2} = f_i^h \tag{A.2}$$

And therefore the discrete operator becomes:

$$L^h \left\langle u^h \right\rangle_i = \frac{u_{i-1}^h + p_i^h u_i^h + u_{i+1}^h}{\Delta x^2}, \qquad i = 1, \ldots, n-1 \tag{A.3}$$

This way a system of equations can be constructed for $\mathbf{u}^h$ resulting in:

$$\mathbf{A} \cdot \mathbf{u}^h = \mathbf{f}^h \tag{A.4}$$

In this equation $\mathbf{A}$ is constructed from the discrete Helmholtz equation and from the boundary conditions. There are different boundary conditions possible for differential equations. Two common boundary conditions are Neumann and Dirichlet boundary conditions. First Dirichlet boundary conditions will be considered, as these will be used in the current application.

For Dirichlet boundary conditions the unknowns are $\left[u_1 \cdots u_{n-1}\right]$ and the left hand side of the system of equations becomes:

$$\frac{1}{\Delta x^2}\begin{bmatrix} \Delta x^2 & 0 & & & & & \\ 1 & p_1^h & 1 & 0 & & & \\ 0 & 1 & p_2^h & 1 & 0 & & \\ & & & \ddots & & & \\ & & 0 & 1 & p_{n-2}^h & 1 & 0 \\ & & & 0 & 1 & p_{n-1}^h & 1 \\ & & & & & 0 & \Delta x^2 \end{bmatrix} \cdot \begin{pmatrix} u_0^h \\ u_1^h \\ u_2^h \\ \vdots \\ u_{n-2}^h \\ u_{n-1}^h \\ u_n^h \end{pmatrix} \tag{A.5}$$

With right hand side:

$$\begin{pmatrix} U_0 \\ f_1^h \\ f_2^h \\ \vdots \\ f_{n-2}^h \\ f_{n-1}^h \\ U_n \end{pmatrix} \tag{A.6}$$

As the values of u_0^h and u_n^h follow directly from the boundary conditions it can be chosen to implement these in the right hand side resulting in $f_1^h - \frac{U_0}{\Delta x^2}$ for one boundary and $f_{ii-1}^h - \frac{U_{ii}}{\Delta x^2}$ on the other side. This does not change the principle of the relaxation process used.

The difference between the left hand side and the right hand side is called the residue and the system is stated to be converged when the residue has reached machine accuracy. Also when the exact solution of the system of equations is used the residue should be zero. Therefore the residue is:

$$r_i^h = f_i^h - L\left\langle \hat{u}^h \right\rangle_i^h \tag{A.7}$$

For an iterative method, the new solution $\hat{u}_i^h$ will be calculated by adding a correction to the old solution $\tilde{u}_i^h$. For the first iteration sweep the old solution will be an appropriate initial guess, after that the new solution of one sweep will become the old solution for the next sweep. This leads to:

$$\hat{u}_i^h = \tilde{u}_i^h + \omega \delta_i^h \tag{A.8}$$

With ω the relaxation factor.

For Gauß-Seidel relaxation δ_i^h is described by:

$$\delta_i^h = \left(\frac{\partial L^h \left\langle u_i^h \right\rangle}{\partial u_i^h} \right)^{-1} r_i^h \tag{A.9}$$

And in this relaxation method the new solution is used in the calculation of the new solution of the next point. This leads to:

$$\hat{u}_i^h = \tilde{u}_i^h + \omega \frac{\Delta x^2}{p_i^h} \left(f_i^h - \frac{1}{h^2} \left(\hat{u}_{i-1}^h + p_i^h \tilde{u}_i^h + \tilde{u}_{i+1}^h \right) \right), \quad i = 1, \ldots, n-1 \tag{A.10}$$

With Neumann or Robin boundary conditions the inner Gauß-Seidel relaxation remains the same.However, equations for u_0^h and u_n^h have to be solved. With central differences a ghost cell will be introduced to derive this equation. The BC states:

$$\frac{\partial u}{\partial x} = g \tag{A.11}$$

Discretized with a central difference scheme this gives:

$$\begin{aligned} \frac{u_1^h - u_{-1}^h}{2\Delta x} &= g_0 \\ \frac{u_{n+1}^h - u_{n-1}^h}{2\Delta x} &= g_n \end{aligned} \tag{A.12}$$

This leads to:

$$\hat{u}_0^h = \tilde{u}_0^h + \omega \frac{\Delta x^2}{p_0^h} \left(f_0^h - \frac{1}{\Delta x^2} \left(p_0^h \tilde{u}_0^h + 2\tilde{u}_1^h - 2\Delta x g_0 \right) \right) \tag{A.13a}$$

$$\hat{u}_n^h = \tilde{u}_n^h + \omega \frac{\Delta x^2}{p_n^h} \left(f_n^h - \frac{1}{\Delta x^2} \left(2\hat{u}_{n-1}^h + p_n^h \tilde{u}_n^h + 2\Delta x g_n \right) \right) \tag{A.13b}$$

A.2 Local Mode Analysis

The Local mode Analysis is used to analyse the reduction of Fourier components of the error obtained by the relaxation. Defining the new error as:

$$\hat{v}_i^h = u_i^h - \hat{u}_i^h \tag{A.14}$$

And the old error as:

$$\tilde{v}_i^h = u_i^h - \tilde{u}_i^h \tag{A.15}$$

Substitution of equations A.14 and A.15 in equation A.10 leads to:

$$\hat{v}_i = (1 - \omega)\, \tilde{v}_i - \omega \frac{\hat{v}_{i-1}^h + \tilde{v}_{i+1}^h}{p_i^h} \tag{A.16}$$

A Fourier series can be constructed for the error made:

$$\hat{v}_i = \sum_{0 < |\theta| \leq \pi} \hat{A}(\theta)\, e^{\iota \theta i} \tag{A.17}$$

and

$$\tilde{v}_i = \sum_{0<|\theta|\leq\pi} \tilde{A}(\theta) e^{\iota\theta i} \tag{A.18}$$

Substituting the Fourier series in equation A.16 gives:

$$\hat{A}(\theta)\left(\frac{\omega}{p_i}e^{-\iota\theta}+1\right) = \tilde{A}(\theta)\left(1-\omega-\frac{\omega}{p_i}e^{\iota\theta}\right) \tag{A.19}$$

Thus:

$$\frac{\hat{A}(\theta)}{\tilde{A}(\theta)} = \frac{p_i(1-\omega)-\omega e^{\iota\theta}}{p_i^h+\omega e^{-\iota\theta}} \tag{A.20}$$

And thus for $\omega = 1$:

$$\mu\left(\theta, p_i^h\right) = \frac{\left|\hat{A}(\theta)\right|}{\left|\tilde{A}(\theta)\right|} = \frac{1}{\left|p_i^h + e^{-\iota\theta}\right|} \tag{A.21}$$

And rewriting the denominator leads to:

$$\mu\left(\theta, p_i^h\right) = \frac{1}{\sqrt{{p_i^h}^2 + 2p_i^h\cos(\theta)+1}} \tag{A.22}$$

For $k = 0$ this equation changes in the Poisson problem with $\mu(0) = 1$. To find a theoretical convergence rate for small θ a Taylor series can be obtained around $\theta = 0$ for $\theta = \mathcal{O}(\Delta x)$:

$$\mu(\Delta x) = 1 - 2\Delta x^2 + \mathcal{O}\left(\Delta x^4\right) \tag{A.23}$$

Therefore the convergence rate for Gauß-Seidel relaxation for the Poisson problem is $1 - \mathcal{O}(\Delta x^2)$.

Appendix B

Kaczmarz for 1D-Helmholz

B.1 Derivation of the relaxation process

Kaczmarz relaxation solves the discrete Helmholtz equation, equation A.2, in a similar way as Gauß-Seidel relaxation. It therefore also solves the system of equations $\mathbf{A} \cdot \mathbf{u} = \mathbf{f}$ with $\mathbf{A}$ and $\mathbf{f}$ for Dirichlet boundary conditions from respectively A.5 and A.6. Kaczmarz will however not directly solve $\mathbf{u}$ but it will do Gauß-Seidel relaxation for $\mathbf{y}$ with:

$$\mathbf{u}^h = \mathbf{A}^T \cdot \mathbf{y}^h \tag{B.1}$$

$\mathbf{A}^T$ follows directly from A.5:

$$\frac{1}{\Delta x^2}\begin{bmatrix}
\Delta x^2 & 1 & 0 & & & & & & \\
0 & p_1^h & 1 & 0 & & & & & \\
0 & 1 & p_2^h & 1 & 0 & & & & \\
 & 0 & 1 & p_3^h & 1 & 0 & & & \\
 & & & & \ddots & & & & \\
 & & & 0 & 1 & p_{n-3}^h & 1 & 0 & \\
 & & & & 0 & 1 & p_{n-2}^h & 1 & 0 \\
 & & & & & 0 & 1 & p_{n-1}^h & 0 \\
 & & & & & & 0 & 1 & \Delta x^2
\end{bmatrix} \tag{B.2}$$

The system to be solved then becomes:

$$\left(\mathbf{A} \cdot \mathbf{A}^T\right) \cdot \mathbf{y}^h = \mathbf{f}^h \tag{B.3}$$

with:

$$\Delta x^4 \mathbf{A}\cdot\mathbf{A}^T =$$

$$\begin{bmatrix}
\Delta x^4 & \Delta x^2 & 0 & & & & & \\
\Delta x^2 & p_1^2+1 & p_1+p_2 & 1 & 0 & & & \\
0 & p_1+p_2 & p_2^2+2 & p_2+p_3 & 1 & 0 & & \\
0 & 1 & p_2+p_3 & p_3^2+2 & p_3+p_4 & 1 & & \\
 & 0 & 1 & p_3+p_4 & p_4^2+2 & & & \\
 & & 0 & 1 & \ddots & \ddots & & \\
 & & & 0 & & & & \\
 & & & & & & \Delta x^2 & \\
 & & & & & & \Delta x^2 & \Delta x^4
\end{bmatrix} \tag{B.4}$$

Gauß-Seidel relaxation will be performed for the new system of equations to solve $\mathbf{y}^h$. For $j = 3,\ldots,n-3$:

$$\hat{y}_i^h = \tilde{y}_i^h + \omega\left(\frac{\partial \mathbf{A}\cdot\mathbf{A}^T}{\partial \tilde{y}_i^h}\right)^{-1}\frac{1}{\Delta x^4}\left(\Delta x^4 f_i^h - \left(\hat{y}_{i-2}^h + \left(p_{i-1}^h + p_i^h\right)\hat{y}_{i-1}^h + \left(p_i^{h\,2}+2\right)\tilde{y}_i^h + \left(p_i^h + p_{i+1}^h\right)\tilde{y}_{i+1}^h + \tilde{y}_{i+2}^h\right)\right) \tag{B.5}$$

With:

$$\frac{\hat{y}_{i-2}^h + \left(p_{i-1}^h + p_i^h\right)\hat{y}_{i-1}^h + \left(p_i^{h\,2}+2\right)\tilde{y}_i^h + \left(p_i^h + p_{i+1}^h\right)\tilde{y}_{i+1}^h + \tilde{y}_{i+2}^h}{\Delta x^4} = \frac{\tilde{\tilde{u}}_{i-1}^h + p_i^h\tilde{\tilde{u}}_i^h + \tilde{\tilde{u}}_{i+1}^h}{\Delta x^2} \tag{B.6}$$

For $i = 2$ and $i = n-2$ the relaxation operator can also be rewritten to $\frac{1}{\Delta x^2}\tilde{\tilde{u}}_{i-1}^h + p_i^h\tilde{\tilde{u}}_i^h + \tilde{\tilde{u}}_{i+1}^h$. Thus for $i = 2,\ldots,i-2$:

$$\hat{y}_i^h = \tilde{y}_i^h + \omega\frac{\Delta x^4}{p_i^{h\,2}+2}\left(f_i^h - \frac{\tilde{\tilde{u}}_{i-1}^h + p_i^h\tilde{\tilde{u}}_i^h + \tilde{\tilde{u}}_{i+1}^h}{\Delta x^2}\right) \tag{B.7}$$

By recognizing the part between parentheses as the residual, this gives:

$$\hat{y}_i^h = \tilde{y}_i^h + \omega\frac{\Delta x^4}{p_i^{h\,2}+2}r_i^h \tag{B.8}$$

With the solutions for $\mathbf{y}^h$ the new $\tilde{\mathbf{u}}^h$ can be calculated. Every calculated y_i^h results in a change of u_{i-1}^h, u_i^h and u_{i+1}^h. These values have to be changed

accordingly and the new values have to be used in the calculation of y_{i+1}^h. Thus in every step δ_i^h becomes:

$$\delta_i^h = \omega \Delta x^2 \frac{r_i^h}{{p_i^h}^2 + 2} \tag{B.9}$$

With:

$$r_i^h = f_i^h - \frac{\tilde{\tilde{u}}_{i-1}^h + p_i^h \tilde{\tilde{u}}_i^h + \tilde{\tilde{u}}_{i+1}^h}{\Delta x^2} \tag{B.10}$$

And the contributions to $\hat{\tilde{u}}^h$ are:

$$\begin{aligned} \hat{\tilde{u}}_{i-1}^h &= \tilde{\tilde{u}}_{i-1}^h + \delta_i^h \\ \tilde{\tilde{u}}_i^h &= \tilde{\tilde{u}}_i^h + p_i^h \delta_i^h \,, \qquad i = 2, \ldots, n-2 \\ \tilde{\tilde{u}}_{i+1}^h &= \tilde{\tilde{u}}_{i+1}^h + \delta_i^h \end{aligned} \tag{B.11}$$

The boundaries need special attention with Kaczmarz relaxation. In the original Gauß-Seidel relaxation the boundary condition only influenced one point. Now however there is a condition for the combination of the boundary and its next point. To solve this problem, the first relation with y_0^h and y_1^h is substituted in the second relation with y_0, y_1 and y_2. And for the end boundary a same construction will be used. This leads to:

$$L\left\langle y_1^h \right\rangle = \frac{\Delta x^2 U_0 + \left(1 + p_1^2\right) y_1^h + \left(p_1 + p_2\right) y_2^h + y_3^h}{\Delta x^4}$$

And thus:

$$\begin{aligned} \delta_1 &= \omega \frac{\Delta x^2 r_1^h}{1 + p_1^2} \\ \delta_{n-1} &= \omega \frac{\Delta x^2 r_{n-1}^h}{1 + p_{n-1}^2} \end{aligned} \tag{B.12}$$

The corrections to be done then become:

$$\begin{aligned} \tilde{\tilde{u}}_1^h &= \tilde{\tilde{u}}_1^h + p_1 \delta_1 \\ \tilde{\tilde{u}}_2^h &= \tilde{\tilde{u}}_2^h + \delta_1 \end{aligned} \tag{B.13}$$

at the beginning of the sweep, and at the end of the sweep:

$$\begin{aligned} \hat{\tilde{u}}_{n-2}^h &= \hat{\tilde{u}}_{n-2}^h + \delta_{n-1} \\ \hat{\tilde{u}}_{n-1}^h &= \tilde{\tilde{u}}_{n-1}^h + p_{n-1} \delta_{n-1} \end{aligned} \tag{B.14}$$

B.2 Local mode analysis

The residual of the solution is calculated with:

$$\mathbf{r}^h = \mathbf{f}^h - \mathbf{A}\mathbf{A}^T\hat{\mathbf{y}}^h \tag{B.15}$$

And the error for $\mathbf{y}^h$ is directly related to the error for $\mathbf{u}^h$ with:

$$\mathbf{v}^h = \mathbf{A}^T \cdot \mathbf{x}^h \tag{B.16}$$

The error for $\hat{y}_i^h$ can be defined in a similar way as the error for u_i^h, and is written as:

$$\hat{x}_i^h = y_i^h - \hat{y}_i^h \tag{B.17}$$

And the error for $\tilde{y}^h$ as:

$$\tilde{x}_i^h = y_i^h - \tilde{y}_i^h \tag{B.18}$$

Substitution of the error in the relaxation operator gives:

$$\begin{aligned}\hat{x}_i^h + \frac{\omega}{{p_i^h}^2+2}\left(\hat{x}_{i-2}^h + \left(p_{i-1}^h + p_i^h\right)\hat{x}_{i-1}^h\right)& \\ = \tilde{x}_i^h - \frac{\omega}{{p_i^h}^2+2}\left(\left({p_i^h}^2+2\right)\tilde{x}_i^h + \left(p_i^h + p_{i+1}^h\right)\tilde{x}_{i+1}^h + \tilde{x}_{i+2}^h\right)&\end{aligned} \tag{B.19}$$

A Fourier series can be constructed for the error, leading to:

$$\begin{aligned}\hat{v}_i^h = \sum_{0<|\theta|\leq\pi}\hat{A}(\theta)e^{\iota\theta i} = \hat{x}_{i-1} + p_i^h\hat{x}_i + \hat{x}_{i+1}& \\ = \left(e^{-\iota\theta i} + p_i^h + e^{\iota\theta i}\right)\sum_{0<|\theta|\leq\pi}\hat{B}(\theta)e^{\iota\theta i}&\end{aligned} \tag{B.20}$$

and

$$\begin{aligned}\tilde{v}_i = \sum_{0<|\theta|\leq\pi}\tilde{A}(\theta)e^{\iota\theta i} = \tilde{x}_{i-1} + p_i^h\tilde{x}_i + \tilde{x}_{i+1}& \\ = \left(e^{-\iota\theta i} + p_i^h + e^{\iota\theta i}\right)\sum_{0<|\theta|\leq\pi}\tilde{B}(\theta)e^{\iota\theta i}&\end{aligned} \tag{B.21}$$

Substituting the Fourier series in equation B.19 gives:

$$\begin{aligned}\hat{B}(\theta)\left(1 + \frac{\omega}{{p_i^h}^2+2}\left(e^{-2\iota\theta} + \left(p_{i-1}^h + p_i^h\right)e^{-\iota\theta}\right)\right)& \\ = \tilde{B}(\theta)\left(1 - \omega - \frac{\omega}{{p_i^h}^2+2}\left(\left(p_i^h + p_{i+1}^h\right)e^{\iota\theta} + e^{2\iota\theta}\right)\right)&\end{aligned} \tag{B.22}$$

Using the errors defined in equations B.20 and B.21 and using equation B.22, the ratio can be determined for the new error with respect to the former error:

$$\frac{\hat{A}(\theta)}{\tilde{A}(\theta)} = \frac{e^{-\iota\theta} + p_i^h + e^{\iota\theta}}{e^{-\iota\theta} + p_i^h + e^{\iota\theta}} \frac{\hat{B}(\theta)}{\tilde{B}(\theta)} = \frac{\hat{B}(\theta)}{\tilde{B}(\theta)}$$
$$= \frac{\left(p_i^{h2} + 2\right)(1-\omega) - \omega\left(\left(p_i^h + p_{i+1}^h\right)e^{\iota\theta} + e^{2\iota\theta}\right)}{p_i^{h2} + 2 + \omega\left(e^{-2\iota\theta} + \left(p_{i-1}^h + p_i^h\right)e^{-\iota\theta}\right)} \tag{B.23}$$

With $\omega = 1$ the residual reduction factor in equation B.23 becomes:

$$\mu\left(\theta, p_i^h\right) = \frac{\left|\hat{A}(\theta)\right|}{\left|\tilde{A}(\theta)\right|} = \frac{\left|e^{\iota\theta}\left(p_i^h + p_{i+1}^h + e^{\iota\theta}\right)\right|}{\left|p_i^{h2} + 2 + e^{-2\iota\theta} + \left(p_{i-1}^h + p_i^h\right)e^{-\iota\theta}\right|} \tag{B.24}$$

When the wave number is constant, equation B.24 changes in:

$$\mu\left(\theta, p\right) = \frac{\left|2p + e^{\iota\theta}\right|}{\left|\left(e^{-\iota\theta} + p\right)^2 + 2\right|} \tag{B.25}$$

For $k = 0$ the problem changes to the Poisson problem with $\mu(0) = 1$. To determine the convergence rate for single grid relaxations the convergence rate can be approximated by $\mu(\Delta x)$. For small Δx a Taylor series can be constructed around $\theta = 0$. While a Taylor series for an arbitrary wave number produces a second order dependency on Δx, the second order term is zero for $p = -2$. This leads to the following expansion for $k = 0$:

$$\mu(\Delta x) = 1 - \frac{1}{3}\Delta x^4 + \mathcal{O}\left(\Delta x^6\right) \tag{B.26}$$

Thus the convergence rate is $1 - \mathcal{O}(\Delta x^4)$ and is for small h very slow with respect to $1 - \mathcal{O}(\Delta x^2)$ for Gauß-Seidel relaxation for the Poisson problem.